Multimodal cell lineage reconstruction in the hindbrain reveals a link between progenitor origin and activity patterning

Matthias Blanc[1,3*], Lydvina Meister[1], William C. Lemon[2], Ulla-maj Fiuza[1], Philipp J. Keller[2], Isabel Espinosa-Medina[2,*], Cristina Pujades[1,4,*]

[1]Department of Medicine and Life Sciences, Universitat Pompeu Fabra, 08003 Barcelona, Spain

[2]HHMI Janelia Research Campus, Ashburn, VA 20147, US

[3]Current address: Institute for Stem Cell Biology and Regenerative Medicine, Stanford University

[4]Lead contact

[*]Correspondence: Matthias Blanc mblanc@stanford.edu
Isabel Espinosa-Medina espinosamedinai@janelia.hhmi.org
Cristina Pujades cristina.pujades@upf.edu

KEYWORDS (up to 10): cell lineage, proneural genes, neural progenitors, neuronal differentiation, excitatory glutamatergic neurons, inhibitory GABAergic neurons, zebrafish, morphogenesis, hindbrain

ABSTRACT 157w

Does the stem cell origin impact how daughter neurons acquire functional characteristics and assemble into circuits? Here, by multimodal cell lineage reconstruction in the zebrafish hindbrain we related a neuron's embryonic origin to its future terminal differentiation features, such as neurotransmitter identity, and neuronal activity pattern. Intersectional lineage tracing, new developed computational tools, and genetic knockouts revealed that different progenitors formed functionally distinct neuron subtypes and could not compensate for the loss of adjacent progenitor pools, indicating developmental hardwiring. Dynamics of neuronal production suggest that progenitor competence changes over time. Whereas *neurog1*-expressing progenitors contributed to both glutamatergic and GABAergic lineages at early embryonic stages, later, other progenitor pools also assumed this role. Whole-hindbrain 3D atlases combining calcium imaging to monitor spontaneous neuronal activity, with genetic perturbations and progenitor origin information, unveiled that the emergence of neuronal activity patterns was presaged by their progenitor origins. This reveals a link between cell ontogeny and neuronal activity in the zebrafish hindbrain.

MAIN

The survival of an organism requires the constant coordination of the activities of its organs with the ever-changing external environment that it encounters. The responsibility for these tasks falls on the neuronal circuits, which are generated during embryonic development, and critically reflect the structural and functional organization of the emerging network[1,2]. A fundamental question is how the variety of neuronal activity patterns displayed by the extraordinary diversity of neuronal types is established during embryonic development. While much is known about how neurons are generated[3], the variables that drive a seemingly uniform pool of neural progenitor cells into the specific functional neuronal types in a temporally coordinated manner are still not clear.

Here, we explore this issue in the context of the zebrafish hindbrain and find that a neuron's embryonic progenitor origin foreshadows both its terminal differentiation features, such neurotransmitter identity, and the acquisition of spontaneous activity pattern. We tackled this in the hindbrain because it is highly conserved along evolution[4] and it harbors 80% of the total brain neurons[5], which are produced extremely rapidly at early embryonic stages[6,7]. These neurons establish early functional circuits, which are essential for fundamental physiological responses/behaviors such as respiration, circulation, arousal and movement[8–10]. Thus, the hindbrain is uniquely suited to study how temporal control and progenitor competence are coupled.

During embryonic development, several cell types are known to originate from more than one source. Spatial cues regulating cell fate decisions have been established[11,12]. The most studied example is the spinal cord, where over a dozen different neural progenitor types are spatially arrayed along the dorsoventral axis to give rise the distinct neuronal fates[13,14]. However, temporal mechanisms also play a large role in controlling progenitor competence. For instance, cortical progenitors mature over time such that we find inverted temporal gradients of "early" vs. "late" genes[15], and neural progenitors gradually switch from specifying earlier-born cell fates to specifying later-born neurons[15–17]. In the hindbrain, the spatial distribution of neurons in the tissue foreshadows the time of neuronal differentiation, with an inner–outer gradient[7] in which cells born first are more innerly located than cells born last, and neuronal birthdate is important in ascribing neuronal function[18,19]. These observations raise the question whether both progenitor origin and order of neuronal differentiation confer specific

neuronal activity patterns. Addressing how this occurs has been technically challenging to date since it is difficult to trace the origin of functional neurons while recording their spontaneous activity. However, the zebrafish hindbrain offers excellent experimental suitability since its transparency and small size allow high-resolution live imaging and genetic lineage tracing at whole-organ scale, while genome editing enables precise perturbations.

Here, we present a multimodal approach to address the role of the spatiotemporally defined progenitor origin in the construction of excitatory (glutamatergic) and inhibitory (GABAergic) networks leading to the emergence of spontaneous neuronal activity. By combining progenitor intersectional fate mapping[20] and CRISPR-based perturbation experiments with a new computational pipeline to generate 3D reference maps of whole brains, we establish the differential temporal contribution of distinct progenitor pools –defined by proneural gene expression– to the glutamatergic and GABAergic lineages. We find that whereas *neurog1*-expressing progenitors contribute to both glutamatergic and GABAergic lineages in early embryonic stages, later, other proneural gene-expressing progenitor pools either also assume this role (for glutamatergic neurons) or take over (for GABAergic neurons). Further, by using 3D spatial correlation and calcium imaging to record neuronal activity in the entire developing circuit we unveil that cell lineage origin is crucial in defining neuronal activity. Finally, by performing calcium recordings upon perturbation of distinct progenitor pools we demonstrate that temporally defined progenitor origin determines specific functional neuronal features: early-born, medially located progenitors produce neurons characterized by high-amplitude, low-frequency, and synchronized activity, likely establishing the baseline circuit architecture; by contrast, later-born, laterally located progenitors produce neurons with low-amplitude, high-frequency, and asynchronous activity, suggesting a role in more specific fine-tuning. Thus, both progenitor origin and age are crucial parameters in establishing terminal characteristics, such as neurotransmitter identity and function, demonstrating that the lineage and developmental trajectory of a cell are key determinants of cellular functional identity.

RESULTS

To reveal how spatial neurogenesis patterns are established in the hindbrain, we first assessed the temporal expression of proneural genes (PN) –transcription factors that commit progenitors towards the neuronal lineage– in the neural progenitor domain. At 24hpf, their expression differed along the dorsoventral (DV) axis (Figure 1a–e), with 5 distinct progenitor pools defined according to the PN-gene combinations. While most progenitor pools' distribution was similar to that of the spinal cord[21,22], the most dorsal *neurog1* expression domain was absent (Figure 1a, e). *neurog1*-expressing progenitors were mainly, but not exclusively, contained within the *ascl1b*-domain (Figure 1a–b, e), whereas *ptf1a* and *atoh1a* progenitors were segregated to the dorsal-most part of the tissue with no observable overlap with other PN genes (Figure 1c–e; [23]). Progenitors placed in the dorsal domain at 24hpf were located dorsolateral at 48hpf due to the progressive opening of the neural tube (Figure 1f–j). By 48hpf, most of the *neurog1*-domain was still contained within the *ascl1b*-region (Figure 1f–g, j), which expanded laterally towards the *ptf1a*-domain (Figure 1g–h, j). This change in the temporal PN expression profile may result in part from two intertwined morphogenetic events that occur during development, the growth of the neuronal differentiation domain at the expense of the progenitor territory[7,24] and the formation of the brain lumen[23–25]. The expression of PN genes along the anteroposterior (AP) axis differed (Extended Data Figure 1a–j). At 24hpf, *ascl1b* was expressed all along the AP axis in a ventral domain comprising *neurog1* (see dorsal views in Extended Data Figure 1 a–b, e; a'–b', e') and only in the posterior hindbrain in a specific dorsal domain comprised between the *ptf1a* and *atoh1a* domains (Figure 1b, e). By 48hpf, this dorsally located *ascl1b* domain displayed *neurog1* as well, while still being absent in more anterior regions (Figure 1f–g, j; Extended Data Figure 1f–f', j–j'). Overall, these results show that PN genes dynamically pattern the neural progenitor domain (Figure 1k).

Next, to monitor the growth of the *neurog1*-progenitor pool we built up the Tg[*neurog1*:Cre-P2a-nlsCerulean] transgenic zebrafish line, with Cre under the control of *neurog1* promoter. In transgenic embryos, *neurog1* mRNA expression was restricted to the progenitor domain (Extended Data Figure 2a–c, a'–c'), and accordingly, HCR analysis revealed overlapping expression of *Cre* and *neurog1* (Extended Data Figure 2d–d'', e–e''). *In vivo* Light Sheet Fluorescence Microscopy (LSFM) imaging of Cerulean expression demonstrated this new

transgenic line faithfully recapitulates the expected neurog1 spatiotemporal patterning during hindbrain morphogenesis (Extended Data Figure 2f–j, f'–j').

neurog1-progenitors differentially contribute to excitatory and inhibitory neurons with distinct temporal dynamics

We explored the differential temporal contribution of distinct PN-expressing progenitor pools to the excitatory (glutamatergic) and inhibitory (GABAergic) neuronal circuits (Figure 1l), which constitute 80% of the overall hindbrain neurons born before 72hpf[24]. We used progenitor-restricted intersectional mapping[20] to singularize cell lineages arising from specific progenitor populations and assessed their temporal contribution to the differentiated neuronal derivatives (Figure 1l).

To address the contribution of *neurog1*-progenitors to the specific glutamatergic (*vglut2a*) or GABAergic (*gad1b*) neuronal subsets, Tg[*neurog1*:Cre-P2a-nlsCerulean] fish (hereafter Tg[*neurog1*:Cre]) were crossed with Tg[*vglut2a/gad1b*:Lox-DsRed-Lox-GFP] fish[26] (hereafter Tg[*vglut2a/gad1b*:switch]) and the resulting embryos were *in vivo* imaged during periods encompassing the beginning of neuronal differentiation (24hpf) until most of the hindbrain cells are postmitotic neurons (72hpf)[7,24]. The production of glutamatergic and GABAergic neurons followed distinct dynamics with several progenitor pools contributing to their growth (Figure 1m–o, p–r; see *neurog1*-derived cells in green and the ones derived from other progenitors in magenta). *neurog1*-progenitors generated both types of differentiated neurons; while glutamatergic derivatives were already widely present in the hindbrain by 24hpf (see green cells in Figure 1m, m') the only few GABAergic neurons at that stage derived from *neurog1*-cells and corresponded to sensory ganglia outside the hindbrain[27,28] (see white arrow in Figure 1p, p'). By 48hpf, although *neurog1*-progenitors were still contributing to glutamatergic neurons, other PN-expressing progenitors started contributing to their production (see magenta cells in Figure 1n, n') and this was maintained by 72hpf (Figure 1o, o'). On the other hand, by 48hpf most of GABAergic neurons derived from *neurog1*-progenitors (see green cells in Figure 1q, q'), and by 72hpf, GABAergic neurons were contributed strongly by other progenitor pools (see magenta cells in Figure 1r, r'). To further address the progenitor contribution dynamics, we performed LSFM recordings and observed two distinct behaviors for these neurotransmitter's defined subsets. Glutamatergic neurons were simultaneously and consistently produced by both *neurog1*-expressing progenitors and

other pools across development, whereas GABAergic neurons were exclusively produced by *neurog1*-progenitors early on, and later they were generated by other contributors (Extended Data Videos 1–4). Although the secondary production of GABAergic neurons was initiated later, it resulted in the production of a relatively similar proportion of neurons (Extended Data Videos 3–4). These results demonstrate a differential temporal growth of glutamatergic and GABAergic hindbrain neurons, with distinct spatiotemporal contribution of progenitor pools. Whereas *neurog1*-progenitors contribute to both lineages in early embryonic stages, later, other progenitor pools either also assume this role (for excitatory neurons), or take over (for inhibitory neurons). Next, we wanted to identify the other progenitor pools contributing to these lineages.

Glutamatergic and GABAergic lineages derive from distinct progenitor pools combinations

To resolve the heterogeneity of contributors and identify them, we combined progenitor-restricted intersectional mapping using the Tg[*neurog1*:Cre] and the Tg[*vglut2a*/*gad1b*:switch] lines with a CRISPR/Cas9-based approach that produces loss-of-function (LOF) phenotypes in F_0 by redundantly targeting single genes[29,30] –and therefore impair the formation of specific progenitor pools. Either *neurog1*, *ascl1b*, *ptf1a* or *atoh1a* proneural genes were targeted by injecting one cell stage embryos with four different gRNA per proneural gene (Extended Figure Data 3a–c), and we assessed the impact *i)* on the expression of PN genes in the adjacent domains by HCR-multiplex transcript analysis (Figure 2a; Extended Figure Data 3d–m) and *ii)* on the glutamatergic and GABAergic lineages (Figure 2b). *neurog1*_gRNA injections resulted in smaller hindbrains with no dramatic changes in adjacent PN gene expression (Extended Data Figure 3d–e, i–j), although there was an upregulation of *neurog1* in the statoacoustic ganglion as previously reported[27,28] (data not shown). *ascl1b*_gRNA injected embryos displayed smaller hindbrains with a smaller *neurog1* territory (Extended Data Figure 3d, f, i, k) suggesting a regulation of *neurog1* by *ascl1b*. *ptf1a*_gRNA resulted in an expansion of *ascl1b* (Extended Data Figure 3d, g, i, l) indicating that *ptf1a- and ascl1b*-domains interact. Finally, *atoh1a*_gRNA did not dramatically impact the adjacent *ptf1a* domain (Extended Data Figure 3d, h, i, m) showing that there was no cross-regulation as previously demonstrated in the *atoh1a*^{fh282} mutants[23].

Next, we analyzed the impact of proneural gene LOF on the glutamatergic and GABAergic lineages by 72hpf (Figure 2b). Tg[neurog1:Cre:*vglut2a*/*gad1b*:switch] embryos were injected

with control or PN_gRNAs, imaged at 72hpf, and cell lineages' analyses were performed to *i)* quantify the proportions of glutamatergic and GABAergic neurons derived from the different progenitor populations and *ii)* construct spatial distribution models allowing the evaluation of the impact of LOF on the neuronal populations across the tissue (Figure 2b). To quantify the outcome on the neuronal populations we established a computational workflow combining *i)* a newly generated deep learning-based software, RAD (Rigid Alignment with Deep learning) to perform rigid registration among samples, which enabled supervised or unsupervised alignment of tissues using a trained digital neural network (see https://github.com/cristinapujades/Blanc_et_al_2025), *ii)* the latest version of Cellpose[31], a deep learning single cell segmentation framework, and *iii)* a set of Python scripts to quantify, process and generate representative 3D-models averaging 10 hindbrains per condition including different transgenic backgrounds (Figure 2b). Our averaged 3D-models revealed an important decrease upon *atoh1a* downregulation (Figure 2c, f). Quantification of individual samples showed that the global glutamatergic population was significantly reduced upon *ascl1b* and *atoh1a* LOF and that this reduction was mostly due to a cell population located in the anterior hindbrain (r1-r5) (Figure 2h). A minor reduction was also observed anteriorly upon *ptf1a* LOF, demonstrating an indirect effect of the GABAergic perturbation. The shift in the proportion of *neurog1*-derivatives in the r1-r5 region placed *atoh1a*-progenitors as the major other contributor –besides *neurog1*-progenitors– to the glutamatergic pool (Figure 2i). To spatially map these progenitors, we put forward the depleted and compensated cell subsets across the hindbrain by performing deltas of spatial distribution between control and loss-of-function 3D-models (Extended Data Figure 4a–d). By combining the depleted subset of the various loss-of-function experiments we generated a 3D global model of PN-progenitor requirements for glutamatergic neurons across the hindbrain, which informed us about the spatial requirements for *neurog1*-, *ascl1b*- and *atoh1a*-progenitors within the final neuronal population (Figure 2g). These results indicate that the several progenitor pools that contribute to glutamatergic neurons are not segregated progenitor subsets, except for *atoh1a*-progenitors, indispensable to the dorsolateral neurons (Figure 2g). When non-*neurog1* derivatives were overlapped with the proneural gene requirements' map, the quantifications revealed that this population was significantly enriched in the *atoh1a*-dependent subset, bringing further confirmation that *atoh1a* was the other major contributor to the glutamatergic neuronal population (Figure 2j).

When the same strategy was applied to the GABAergic neurons, we observed a dramatic decrease of the GABAergic population upon downregulation of *ptf1a* (Figure 2k–n). Quantifications revealed a significant reduction of GABA neurons upon both *neurog1* and *ptf1a* LOF (Figure 2p), which was restricted to the anterior hindbrain in the case of *neurog1*_gRNA but was evenly distributed along the AP axis in the context of the *ptf1a*_gRNA (Extended Data Figure 4e–h). To further confirm that the *neurog1*-population was able to produce GABAergic neurons independently of *ptf1a*, we performed LSFM imaging in the cell lineage tracing reporter background and observed that indeed *neurog1*-cells were giving rise to GABAergic neurons in the absence of *ptf1a* (Extended Data Video 5). Moreover, we revealed a decrease in the ratio of *neurog1*-derived neurons upon *ascl1b* LOF in the whole hindbrain with no significant impact on the global GABAergic cell quantity (Figure 2q) unveiling a compensation mechanism and suggesting that at least a subset of the *neurog1*-progenitors is dependent on *ascl1b*. When the progenitors' origin requirement maps were confronted to our lineage tracing models, we further confirmed *ptf1a* to be the most likely major other contributor to the GABAergic lineage (Figure 2o, r). These results back up our previous observation that *neurog1*-progenitors are the main contributors to GABAergic neurons at early stages, and that later, *ptf1a*-progenitors take the relay. Accordingly, the *neurog1*-expression domain located laterally, between the *atoh1a* and the *ptf1a* domains, disappeared upon *ascl1b* or *ptf1a* LOF, as shown by HCR experiments at 48hpf (see asterisk in HCR for *neurog1* in Extended Figure Data 3i, k–m). Overall, these observations suggest that the GABAergic neurons originating from *neurog1*-progenitors derive from two subpopulations, one located medially that is *ptf1a*-independent and one located laterally that is *ptf1a* and *ascl1b* dependent.

Progenitor origin defines early functional patterning of hindbrain neurons

To understand the extent to which the ontogeny of a cell is linked to its function, we first addressed the composition of functional cell populations in the embryonic hindbrain at 72hpf. Since at this stage no neuronal activity recordings were publicly available, we made use of the Tg[*elavl3*:jrGECO1b] transgenic line to record spontaneous activity in the whole hindbrain (Figure 3a; Extended Data Figure 5a) using high-speed simultaneous multi-view light-sheet microscopy (hs-SiMView[32]). To extract single cell information, we developed an image analysis pipeline to establish individual cell profiles of the detectable active neurons across the whole

hindbrain (Figure 3a; Extended Data Figure 5b). We identified 4 communities using Louvain clustering, which displayed high cell-to-cell activity correlations (Figure 3b), and upon UMAP analysis plotted in a segregated manner (Figure 3c). Different neuronal communities displayed specific features (Figure 3d). For instance, each community displayed a different synchronization score, community 4 being by far the less synchronized (Figure 3d; C1 = 0.66, C2 = 0.52, C3 = 0.49, C4 = 0.06). To explore whether neurons and communities displaying different activity patterns were differentially located, we plotted their spatial distribution and revealed that indeed neuronal activity features were specifically allocated within the hindbrain (Figure 3e–g; Extended Data Figure 5f–i). For instance, C4 was the most laterally located community with a particular lack of synchronicity combined with a high number of low amplitude calcium spikes (Figure 3d, g; Extended Data Figure 5i). To seek whether there was a correlation between neuronal activity and cell lineage, we used whole registered zebrafish hindbrain images and compared distinct neuronal differentiation patterns in a unified spatiotemporal reference space[7] (see Methods). This provided a platform to dissect the relationship between structure, gene expression and function in brain networks (Figure 3a). Dissecting the neuronal composition of these communities revealed no cell lineage exclusivity (Figure 3h), hinting at indispensable circuit scale properties of the analyzed derivatives. Nevertheless, there was an enrichment of given lineages in communities displaying widely different activity patterns. When dissecting the composition of communities within the glutamatergic and GABAergic populations deriving from *neurog1*- or non-*neurog1*-progenitors we observed noticeable differences in community configuration. The *neurog1*-derived neurons constituted most of both glutamatergic and GABAergic active populations (Figure 3h; see green and cyan bars in C1–C4; Extended Data Figure 5j, l). Notably, community 2 displaying the highest count of synchronized spikes was enriched in *neurog1*-derived glutamatergic neurons (Figure 3d, see green bars in 3h; Extended Data Figure 5j), and community 3 showing lower count but higher intensity spiking was enriched in *neurog1*-derived GABAergic neurons (Figure 3d, see cyan bars in 3h; Extended Data Figure 5l). On the other hand, community 4 displaying the most variable and least synchronized activity presented the highest proportion of non-*neurog1* derivatives (Figure 3d, see magenta and red bars in 3h; Extended Data Figure 5k, m). Most of the active neurons in all communities were glutamatergic and GABAergic neurons, although there was a small proportion of other neuronal type (Figure 3h, see grey bars). To further identify the potential lineage drivers of the

observed functional features we analyzed the cell lineage requirements of the different communities (Figure 3i). We observed a significant enrichment in the proportion of *atoh1a*-dependent glutamatergic and *ptf1a*-dependent GABAergic neurons attributed to community 4 (Figure 3i; see magenta and blue bars in C4). This observation aligned with our progenitor contribution assessment, which associated community 4 with non-*neurog1* derivatives.

To confirm the association of the *neurog1*-derived neuronal subset to a given synchronicity profile we first analyzed the individual lineage-associated subset community compositions and observed that non-*neurog1* derived glutamatergic and GABAergic populations systematically contained more cells in the unsynchronized community 4 (see C4 in Extended Data Figure 5k, m; with community counts in bold and a black asterisk indicating the corresponding cell-cell synchronicity matrice). Taken together, those distributions suggest a particular progenitor cell origin to the be the source of the observed synchronicity. To prove this, we measured the cell-cell synchronicity scores across the lineage defined derivatives and observed significant differences between *neurog1* and non-*neurog1* derivatives, suggesting *neurog1* derivatives to be specifically associated with synchronized activity (Figure 3h). Finally, after associating a circuit feature to *neurog1*-derivatives we wanted to evaluate if a given lineage could be associated with specific single cell signal features. Although some functional features such as the global synchronicity score relied on the cell lineage (Figure 3j), not all activity features did so (Figure 3k). When we measured spike counts across the recording, we noticed that the glutamatergic neurons dependent on *atoh1a*-progenitors displayed a significant increase in spike count compared to the *ascl1b*-dependent ones, but no differences were observed in GABAergic neurons (Figure 3k). Overall these results demonstrate differences of activity among the lineages indicating a correlation between the lineage and both circuit and signal scale activity features.

To further demonstrate causality between the presence of cell lineage specific populations and the activity patterns observed across the hindbrain, we combined calcium imaging recordings with the CRISPR/Cas9-based loss-of-function approach. We observed major changes in neuronal activity (Figure 4a–e; Extended Data Videos 6–10) such as a decrease in cell-cell activity correlations (i.e synchronicity) upon *ascl1b* loss of function (Figure 4a–c, a'–c'). This was further confirmed by the analysis of the average activity pattern (Figure 4a''–c''), in which *neurog1*_gRNA embryos displayed an overall decrease in signal amplitude with no loss of synchronicity (compare Figure 4a'' and 4b''). *ascl1b*_gRNA embryos showed the highest

standard deviation and lack of temporally defined spiking (compare Figure 4a'' and 4c''). Since *ascl1b* and *neurog1* were expressed in similar domains (Extended Data Figure 3), these results suggest that the synchronicity enrichment in *neurog1*-derived populations depend on *ascl1b*. Neuronal activity upon *ptf1a* loss-of-function resulted in wider spikes without losing circuit-wide synchronicity or amplitude of signal (compare Figure 4a'' and 4d''), with the possibility that the generation of spiking trails could be associated to the direct disruption of spike timings resulting from an imbalanced inhibition[28]. On the contrary, upon *atoh1a* loss-of-function we observed no loss of synchronicity or amplitude of signal, whereas the number of spikes was greatly increased across the whole tissue, although not in the form of spiking trails but as individual events (compare Figure 4a'' and 4e''). Since the *atoh1a*-dependant glutamatergic neurons displaying significantly high spike count constituted the major component of the asynchronous community (C4, Figure 3i), and localized proximally sensory neurons, it is likely that *atoh1a*-derived glutamatergic neurons are involved in decoding the sensory input in the hindbrain.

DISCUSSION

Our research highlights that excitatory and inhibitory neurons originate from different progenitor pools –defined according to proneural gene expression– and provides *in vivo* evidence for a link between neuronal cell ontogeny and function. Moreover, our findings reveal that the spatiotemporal order of neuronal differentiation is essential to establish functional neuronal circuits (Figure 5). Neuronal identity is defined by specific gene expression programs, which are executed by gene regulatory networks[33]. However, the cell lineage history within a given tissue context and temporal progression are emerging as central to defining cell fate, emphasizing that gene expression alone is not enough to explain how neurons with distinct morphologies and functional roles are generated in the central nervous system[12,34].

Our results challenge the prevailing view in vertebrate brain neurogenesis that both excitatory neurons and inhibitory neurons derive from two spatially segregated progenitors that express either *neurog1* (excitatory glutamatergic neurons) or *ptf1* (inhibitory GABAergic neurons)[35,36]. We demonstrate that they instead arise from several progenitor pools. Glutamatergic neurons derive mainly from *neurog1*, *ascl1b* and *atoh1a* progenitors whereas GABAergic neurons derive mainly from *neurog1* and *ptf1a* progenitors. The multiple and distinct sources of glutamatergic and GABAergic neuronal populations suggest the presence of lineage defined subcategories within those populations, as it has been demonstrated in other developmental systems such as the lymphatic vessels[37]. This indicates a certain plasticity of the progenitor pools during development, to maintain the robustness of the system. We further elucidate a crucial temporal component: at early embryonic stages, *neurog1*-expressing progenitors contribute to both lineages; in later stages, other progenitor pools either take over (for inhibitory neurons) or also assume this role (for excitatory neurons). Several works suggested the importance of neuronal age-related patterning in forming a foundation for the construction of the networks underlying the many behaviors produced by the hindbrain[7,18,19]. Now, we provide a clearer picture to the lineage with spatial and temporal drivers leading to the generation of neuronal diversity in the hindbrain, supporting the notion that cell lineage and developmental trajectory are key determinants of cellular identity. Further, we provide *in vivo* models that integrate the *temporal logic* within intact tissue architecture and help us to better interrogate brain development and to pave the way for cell therapies.

The emergence of new and increasingly sophisticated behaviors after birth is accompanied by dramatic increase of newly established synaptic connections in the nervous system. Here we provide the first evidence at the global tissue scale that the cell lineage is pivotal for encoding neuronal function early on, helping to explain how nascent connections are organized to build up new behaviors on top of existing functional circuits. The high reproducibility of neuronal activity patterns indicates the robustness of zebrafish embryo fundamental circuits for survival, in line with other studies showing that functional maturation of neurons is stereotyped, based on birth time and anatomical origin[38]. This does not mean that the early acquired functional features will be maintained up to adulthood; rather, it primarily tells us that neuronal activities crucial for life-sustaining of the individual as those coordinated by the hindbrain are established very early. One of these examples would be the hindbrain V2a neurons, which are necessary for spontaneously occurring swimming as early as 3dpf and display region-specific differences in the ability to elicit or stop swimming (anterior regions being less efficient)[39]. Therefore, we propose a model in which lineage not only encodes neurotransmitter identity but provides functional purpose to neuronal populations. This would be synchronizing for the most medial cells as shown upon disruption of *ascl1b*-progenitors, buffering for the neurons in between since loss of *ptf1a* results in reduced spike frequency and GABA has been shown to control action potential firing[40,41], and decoding for cells in the most lateral domain receiving the sensory inputs. This suggests that the orchestrated spatiotemporal patterning of proneural gene defined progenitors establishes neuronal diversity and circuit function allowing the essential hindbrain resilience and adaptation necessary for its life sustaining functions.

The combination of 3D- and *in vivo* experiments with new computational resources allowed us to build a common framework to globally interrogate the system and address previously inaccessible questions. In the future, combining this 3D lineage and activity map strategy with spatial transcriptomics or proteomics could further unveil the differential mechanisms underlying the formation of specific functional traits.

ONLINE METHODS

Ethics declarations and approval for animal experiments

All procedures were approved by the institutional animal care, the PRBB Ethics Committee in Animal Experimentation and the Departament de Territori i Sostenibilitat (Generalitat of Catalonia) in compliance with the National and European regulations. The PRBB animal facility has the AAALAC International approval B9900073. All the members accessing the animal house must hold the international FELASA accreditation. The Project License covering the proposed work (Ref 10642, GC) pays particular attention to the 3Rs. For the zebrafish work carried out at Janelia Research Campus (HHMI), all experiments were conducted according to the National Institutes of Health (NIH) guidelines for animal research and approved by the Institutional Animal Care and Use Committee of Janelia Research Campus (IACUC).

Zebrafish strains

All zebrafish strains were maintained alternating generations of incrosses and outcrosses with wild type. Embryos were obtained by mating adult fish following standard methods and grown at 28.5ºC. % 1-phenyl-2-thiourea (PTU) (Sigma-Aldrich) was used as an inhibitor of pigmentation from 24hpf onward. The Tg[βactin:HRAS-EGFP] line (termed Tg[CAAX:GFP] herein) expresses GFP in the plasma membrane and was used to label the cell contours[42]. Tg[vglut2a:Lox:DsRed:Lox-GFP] and Tg[gad1b:Lox:DsRed:Lox:GFP] switch lines label glutamatergic and GABAergic neurons, respectively[22]. The Tg[HuC:GFP] line labels differentiated neurons[43]. The Tg[*elavl3*:jrGECO1b] transgenic line is a reporter of neuronal activity[44]. Tg[neurog1:CreP2A-nlsCerulean] transgenic line was generated using Tol2 transgenesis.

CRISPR/Cas9-based approach to target proneural genes in F_0

Four different CRISPR single RNAs guides (sgRNAs) were used to redundantly target proneural genes following[30]. The strategy was to target 4 sites of each proneural gene CDS encompassing the bHLH DNA binding domain sequence to either generate a frame shift or a premature stop codon either prior to the DNA binding sequence or within the DNA binding sequence, or alternatively a complete excision of the DNA binding sequence (Extended Data Figure 3b). As controls, we used sgRNAs not targeting the zebrafish genome designed by randomization of

antibiotic resistance gene sequences. All CRISPR RNAs (crRNAs) were ordered from Integrated DNA Technologies (IDT) (Table S1). One-cell stage embryos were injected with a Cas9/gRNAs mix, containing IDT Alt-R HiFi S.p. Cas9 Nuclease V3 (62μM) and a 4 gRNAs mix made from IDT crRNA and tracrRNA annealing (100μM). Embryos were injected with ~1nl of 9μM RNP with a 1:1 Ratio of Cas9 and gRNA incubated at 37°C for 5min and chilled on ice before injection[30]. Deletion efficiency was assessed by gDNA PCR amplification of injected embryos. Disruption of the CDS was considered complete when no band of the original sequence length was observed, and partial when a faint band of the original sequence length was still visible. Combinations of gRNAs were tested until they led to most of the samples (n=10) displaying complete disruption.

Whole mount Hybridization Chain Reaction

Zebrafish embryos at selected stages were fixed overnight in 4% paraformaldehyde (PFA) at 4 °C, dehydrated through a methanol series (25%, 50%, 75%, 100%), and stored at −20 °C until use. After rehydration, embryos were permeabilized with proteinase K (10 µg/ml in PBST; PBS with 0.1% Tween-20) for 10 min at 24 hpf or 20 min at 48 hpf, followed by post-fixation in 4% PFA for 20 min at room temperature. HCR™ Gold RNA-FISH was performed according to the manufacturer's instructions (Molecular Instruments, Los Angeles, CA). Custom probe sets targeting *neurog1* (X1), *ptf1a* (X2), *atoh1a* (X7), *Cre* (X7), and *asc1b* (X3) were used with corresponding amplifiers (X1–488, X2–546, X7–514, X3–647). Hybridization was carried out overnight, followed by overnight incubation with amplifiers. Embryos were imaged within 3 days using a SP8 Leica inverted confocal microscope.

Confocal imaging of whole mount embryos

Zebrafish embryos were anesthetized with tricaine and mounted dorsally in 1% low melting point agarose with the hindbrain positioned towards the glass-bottom Petri dish (Mattek) at the desired time. Images were acquired with either a Leica SP8 or Stellaris8 system using 20×glycerol immersion objective, HCX PL APO Lambda blue 20×/0.7 argon laser 30%-80%, DPSS 561; Ready Lasers. z-stacks were recorded with 0.57×0.57 × 1.04 µm voxel size. The gain was adjusted to each signal to cover the full range of pixel values, minimize signal to noise ratio and compensate inter-individual variability.

Confocal image processing

Briefly, confocal images were processed using a standardized workflow in which they were 1) deconvoluted using a Richardson-Lucy algorithm and a theoretical PSF, 2) cropped and flipped to be in a consistent orientation and to reduce weight of duplicated images, 3) aligned to a common reference using our rigid alignment software (RAD), 4) segmented at the single cell level using Cellpose[45], 5) masks were intersected to identify cells that strictly expressed Cre prior to the neurotransmitter and cell count was obtained, and 6) masks of 10 embryos were averaged to generate a population spatial distribution 3D model.

Light Sheet Fluorescence Microscopy

For developmental recordings Tg[neurog1:Cre; vglut2/gad1b:switch] embryos anesthetized with tricaine were mounted in 0.35% LMP-agarose within a V-shape chamber filled with fish water. Imaging was performed every 5 min for 24h at 28.5°C on a Viventis microscope using 16x objective. 445nm, 488nm and 560nm channels were simultaneously recorded for 3 embryos every 5 min.

For calcium imaging, Tg[elavl3:jrGeco1b] embryos were screened for the fluorescent transgenic indicators, immobilized by immersion in E3 water containing alpha-bungarotoxin (1mg/mL) for 2min and rinsed in E3 water for 20min until unresponsive to touch[46,47]. Embryos were then embedded in 2% low melting point agarose (Type VII, Sigma-Aldrich) prepared in filtered fish water and encased within a custom-designed glass capillary (2 mm outer diameter, 20 mm length; Hilgenberg GmbH). The agarose encased embryo was then partially extruded out of the capillary to expose the embryo head. The capillary itself was mounted vertically in the imaging specimen chamber of a SiMView light-sheet microscope filled with filtered fish water maintained at 28.5°C, with the dorsal side of the embryo facing the detection objective (Nikon 16x/0.8 NA). A volume of ~800×400×200µm^3 (X×Y×Z) was acquired with a Z spacing of 2.2µm at a rate of 2Hz, using a 5ms exposure time per image and an illumination laser wavelength of 561nm with 4mW beam power and 2.5µm beam diameter at the sample location. Embryos were recorded for 30min.

Calcium Imaging analysis

Each data set was processed with a MATLAB pipeline previously described[48], and then further processed and integrated with our other datasets as follows. Briefly, recordings were first converted from the binary file format enabling such high-speed data acquisition to

conventional .tiff files, a rolling window defined reference of intensity at regular intervals was used for further deltaF/F computations, and finally deltaF/F data sets were filtered using a median filter of kernel 3 to remove noise. Using a Fiji macro, they were cropped to save storage space and simplify downstream processing, as well as re-scaled to standardize their magnification with respect to our confocal datasets. For the resulting recordings, the first frame was then used to perform the alignment and the transformation matrix was then automatically applied to each frame of the recording within our alignment software (RAD). We then generated a projection over the temporal dimension resulting in a 3D stack representing the most intensely active neurons. This stack was then used to perform a single cell segmentation using Cellpose. Then, individual cell masks were used to trace the fluctuations in intensity across time at those coordinates.

Rigid Alignment with Deep Learning (RAD)

To align images from multiple samples and modalities we developed a Python-based interface with integrated neural network and manual 3D rigid registration capabilities. In brief, it leverages the SITK Python library to apply the computed transformation component generated either through a Pytorch based neural network or through manual user input. It offers different possibilities for neural network training, either leveraging manual inputs or a folder of original and pre-aligned images. It is designed to handle the 3D rigid registration of samples batches as well as the drift correction and jitter correction of 3D timeseries. A set of previously aligned images[7] was used to prepare a training dataset containing about 40 combinations of reference and aligned images. The training dataset was further amplified 5-fold using random transformations (within the range of traditional alignment) allowing to largely extend the range of transformations visible to the neural network during training. The trained model was then used to process each alignment, and each registration was observed and manually adjusted within the UI if deemed necessary before being saved. When performing alignment across modality, a first sample was often aligned manually and then used as reference for other samples of that modality to spare the training of a cross-modality model.

Statistics and reproducibility

Cell counts were obtained using single cell segmentation mask from Cellpose. The trained Cellpose model and script used to generate the training dataset are available upon request. Statistical analysis was performed in GraphPad Prism 9. For each quantified experiment, the number of replicates/embryos (n) and P values are indicated in the corresponding Supplementary Tables (Tables S2–S3). The experiments reported here were repeated independently at least three times to generate the analyzed dataset. Data distribution was not assumed to be normal; a homoscedasticity test was performed prior to the statistical test selection. A z-score mediated outlier detection across all measured cell counts was used to rule out samples from an original pool containing from 15 to 13 embryos for each condition and transgenic background. Data analyses were performed using automated procedures without consideration of experimental groups. Data analysis was performed using the same parameters across groups.

ACKNOWLEDGEMENTS

We would like to thank Dulce Real for technical assistance and Dr Daniel Feliciano and members of the Espinosa-Medina's and Pujades' labs for insights and critical discussions. We thank and Dr Kyle Loh for critical reading of the manuscript. We thank the Janelia Visiting Scientist Program for supporting the collaboration between HHMI Janelia Research Campus and UPF labs, and Dr Misha Arehns' lab for sharing the Tg[*elavl3*:jrGECO1b] transgenic line. The authors thank the Advanced Light Microscopy Unit at the CRG where confocal imaging was performed, the Scientific Computing Core Facility (MELIS-UPF), and the Aquatic Core Facilities at both UPF-PRBB and Janelia.

COMPETING INTEREST'S STATEMENT

The authors declare no conflict of interests.

FUNDING

This work was funded by grants PID2021-123261NB-I00 from Ministerio de Ciencia y Universidades (MICIU), Agencia Estatal de Investigación (AEI, DOI: 10.13039/501100011033) and Fondo Europeo de Desarrollo Regional (FEDER) to CP. The Department of Medicine and Life Sciences (UPF) is a Unidad de Excelencia María de Maeztu (CEX2018-000792-M) funded by the AEI. CP is a recipient of ICREA Academia award (Generalitat de Catalunya).

DATA AVAILABILITY

All relevant data can be found within the article and its supplementary information. For more information or any specific tool, you can contact us. All code is freely available in https://github.com/cristinapujades/Blanc_et_al_2025.

AUTHOR CONTRIBUTIONS

Conceptualization: MB, IEM and CP; Methodology: MB, LM, WCL, PK; Investigation and formal analysis: MB; Validation and analysis: MB and CP; Resources: UF, PK; Writing-original draft: MB, IEM and CP; Visualization: MB; Supervision: CP; Project administration: CP; Funding acquisition: IEM and CP.

REFERENCES

1. Spitzer, N. C. Electrical activity in early neuronal development. *Nature* **444**, 707–712 (2006).

2. Blankenship, A. G. & Feller, M. B. Mechanisms underlying spontaneous patterned activity in developing neural circuits. *Nat Rev Neurosci* **11**, 18–29 (2010).

3. Guillemot, F. Spatial and temporal specification of neural fates by transcription factor codes. *Development* **134**, 3771–3780 (2007).

4. Murakami, Y., Uchida, K., Rijli, F. M. & Kuratani, S. Evolution of the brain developmental plan: Insights from agnathans. *Developmental Biology* **280**, 249–259 (2005).

5. Herculano-Houzel, S. The Human Brain in Numbers: A Linearly Scaled-up Primate Brain. *Front. Hum. Neurosci.* **3**, 31 (2009).

6. Baumann, N. *et al.* Regional differences in progenitor metabolism shape brain growth during development. *Cell* (2025) doi:10.1016/j.cell.2025.04.003.

7. Blanc, M., Dalmasso, G., Udina, F. & Pujades, C. A dynamic and expandable digital 3D-atlas maker for monitoring the temporal changes in tissue growth during hindbrain morphogenesis. *eLife* **11**, e78300 (2022).

8. Guthrie, S. Patterning and axon guidance of cranial motor neurons. *Nature Reviews Neuroscience* **8**, 859–871 (2007).

9. Aldinger, K. A., Elsen, G. E., Prince, V. E. & Millen, K. J. Model organisms inform the search for the genes and developmental pathology underlying malformations of the human hindbrain. *Seminars in pediatric neurology* **16**, 155–163 (2009).

10. Kiecker, C. & Lumsden, A. Compartments and their boundaries in vertebrate brain development. *Nature Reviews Neuroscience* **6**, 553–564 (2005).

11. Belmonte-Mateos, C. & Pujades, C. From Cell States to Cell Fates: How Cell Proliferation and Neuronal Differentiation Are Coordinated During Embryonic Development. *Front. Neurosci.* **15**, 781160 (2022).

12. Briscoe, J. & Marin, O. Looking at neurodevelopment through a big data lens. *Science* **369**, (2020).

13. Hernandez-Miranda, L. R., Müller, T. & Birchmeier, C. The dorsal spinal cord and hindbrain: From developmental mechanisms to functional circuits. *Developmental Biology* **432**, 34–42 (2017).

14. Alaynick, W. A., Jessell, T. M. & Pfaff, S. L. SnapShot: Spinal Cord Development. *Cell* **146**, 178-178.e1 (2011).

15. Telley, L. *et al.* Temporal patterning of apical progenitors and their daughter neurons in the developing neocortex. *Science* **364**, eaav2522 (2019).

16. Oberst, P. *et al.* Temporal plasticity of apical progenitors in the developing mouse neocortex. *Nature* **573**, 370–374 (2019).

17. Mi, D. *et al.* Early emergence of cortical interneuron diversity in the mouse embryo. *Science* **360**, 81–85 (2018).

18. Kinkhabwala, A. *et al.* A structural and functional ground plan for neurons in the hindbrain of zebrafish. *Proceedings of the National Academy of Sciences of the United States of America* **108**, 1164–1169 (2011).

19. Pujala, A. & Koyama, M. Chronology-based architecture of descending circuits that underlie the development of locomotor repertoire after birth. *eLife* **8**, 471 (2019).

20. Poulin, J.-F. *et al.* PRISM: A Progenitor-Restricted Intersectional Fate Mapping Approach Redefines Forebrain Lineages. *Developmental Cell* **53**, 740-753.e3 (2020).

21. Dréau, G. L. & Martí, E. Dorsal-ventral patterning of the neural tube: a tale of three signals. *Developmental Neurobiology* **72**, 1471–1481 (2012).

22. Satou, C. *et al.* Transgenic tools to characterize neuronal properties of discrete populations of zebrafish neurons. *Development* **140**, 3927–3931 (2013).

23. Belzunce, I., Belmonte-Mateos, C. & Pujades, C. The interplay of atoh1 genes in the lower rhombic lip during hindbrain morphogenesis. *PLoS ONE* **15**, e0228225 (2020).

24. Hevia, C. F., Engel-Pizcueta, C., Udina, F. & Pujades, C. The neurogenic fate of the hindbrain boundaries relies on Notch3-dependent asymmetric cell divisions. *Cell Rep.* **39**, 110915 (2022).

25. Gutzman, J. H. & Sive, H. Epithelial relaxation mediated by the myosin phosphatase regulator Mypt1 is required for brain ventricle lumen expansion and hindbrain morphogenesis. *Development* **137**, 795–804 (2010).

26. Satou, C., Kimura, Y. & Higashijima, S. i. Generation of Multiple Classes of V0 Neurons in Zebrafish Spinal Cord: Progenitor Heterogeneity and Temporal Control of Neuronal Diversity. *Journal of Neuroscience* **32**, 1771–1783 (2012).

27. Andermann, P., Ungos, J. & Raible, D. W. Neurogenin1 defines zebrafish cranial sensory ganglia precursors. *Developmental Biology* **251**, 45–58 (2002).

28. Sapède, D., Dyballa, S. & Pujades, C. Cell lineage analysis reveals three different progenitor pools for neurosensory elements in the otic vesicle. *The Journal of neuroscience : the official journal of the Society for Neuroscience* **32**, 16424–16434 (2012).

29. Engel-Pizcueta, C., Hevia, C. F., Voltes, A., Livet, J. & Pujades, C. Her9 controls the stemness properties of hindbrain boundary cells. *Development* **152**, (2025).

30. Kroll, F. *et al.* A simple and effective F0 knockout method for rapid screening of behaviour and other complex phenotypes. *eLife* **10**, e59683 (2021).

31. Stringer, C. & Pachitariu, M. Cellpose3: one-click image restoration for improved cellular segmentation. *Nat. Methods* **22**, 592–599 (2025).

32. Liu, Z. & Keller, P. J. Emerging Imaging and Genomic Tools for Developmental Systems Biology. *Developmental Cell* **36**, 597–610 (2016).

33. Davidson, E. H. & Erwin, D. H. Gene Regulatory Networks and the Evolution of Animal Body Plans. *Science* **311**, 796–800 (2006).

34. Shainer, I. *et al.* Transcriptomic neuron types vary topographically in function and morphology. *Nature* **638**, 1023–1033 (2025).

35. Filippi, A., Mueller, T. & Driever, W. vglut2 and gad expression reveal distinct patterns of dual GABAergic versus glutamatergic cotransmitter phenotypes of dopaminergic and noradrenergic neurons in the zebrafish brain. *J Comp Neurology* **522**, 2019–37 (2014).

36. Lundell, T. G., Zhou, Q. & Doughty, M. L. Neurogenin1 expression in cell lineages of the cerebellar cortex in embryonic and postnatal mice. *Dev Dynam* **238**, 3310–3325 (2009).

37. Das, R. N. *et al.* Generation of specialized blood vessels via lymphatic transdifferentiation. *Nature* **606**, 570–575 (2022).

38. Wan, Y. *et al.* Single-Cell Reconstruction of Emerging Population Activity in an Entire Developing Circuit. *Cell* **179**, 355-372.e23 (2019).

39. Kimura, Y. *et al.* Hindbrain V2a Neurons in the Excitation of Spinal Locomotor Circuits during Zebrafish Swimming. *Curr. Biol.* **23**, 843–849 (2013).

40. Gentet, L. J., Avermann, M., Matyas, F., Staiger, J. F. & Petersen, C. C. H. Membrane Potential Dynamics of GABAergic Neurons in the Barrel Cortex of Behaving Mice. *Neuron* **65**, 422–435 (2010).

41. Cain, S. M. *et al.* GABAB receptors suppress burst-firing in reticular thalamic neurons. *Channels* **11**, 574–586 (2017).

42. Dale, R. M. & Topczewski, J. Identification of an evolutionarily conserved regulatory element of the zebrafish col2a1a gene. *Developmental Biology* **357**, 518–531 (2011).

43. Park, H. C. *et al.* Analysis of upstream elements in the HuC promoter leads to the establishment of transgenic zebrafish with fluorescent neurons. *Developmental Biology* **227**, 279–293 (2000).

44. Yang, E. *et al.* A brainstem integrator for self-location memory and positional homeostasis in zebrafish. *Cell* **185**, 5011-5027.e20 (2022).

45. Stringer, C., Wang, T., Michaelos, M. & Pachitariu, M. Cellpose: a generalist algorithm for cellular segmentation. *Nat Methods* **18**, 100–106 (2021).

46. Sheets, L. *et al.* Enlargement of Ribbons in Zebrafish Hair Cells Increases Calcium Currents But Disrupts Afferent Spontaneous Activity and Timing of Stimulus Onset. *J. Neurosci.* **37**, 6299–6313 (2017).

47. Ahrens, M. B., Orger, M. B., Robson, D. N., Li, J. M. & Keller, P. J. Whole-brain functional imaging at cellular resolution using light-sheet microscopy. *Nature Methods* **10**, 413–420 (2013).

48. Lemon, W. C. & Keller, P. J. Live imaging of nervous system development and function using light-sheet microscopy. *Mol. Reprod. Dev.* **82**, 605–618 (2015).

FIGURES

Figure 1

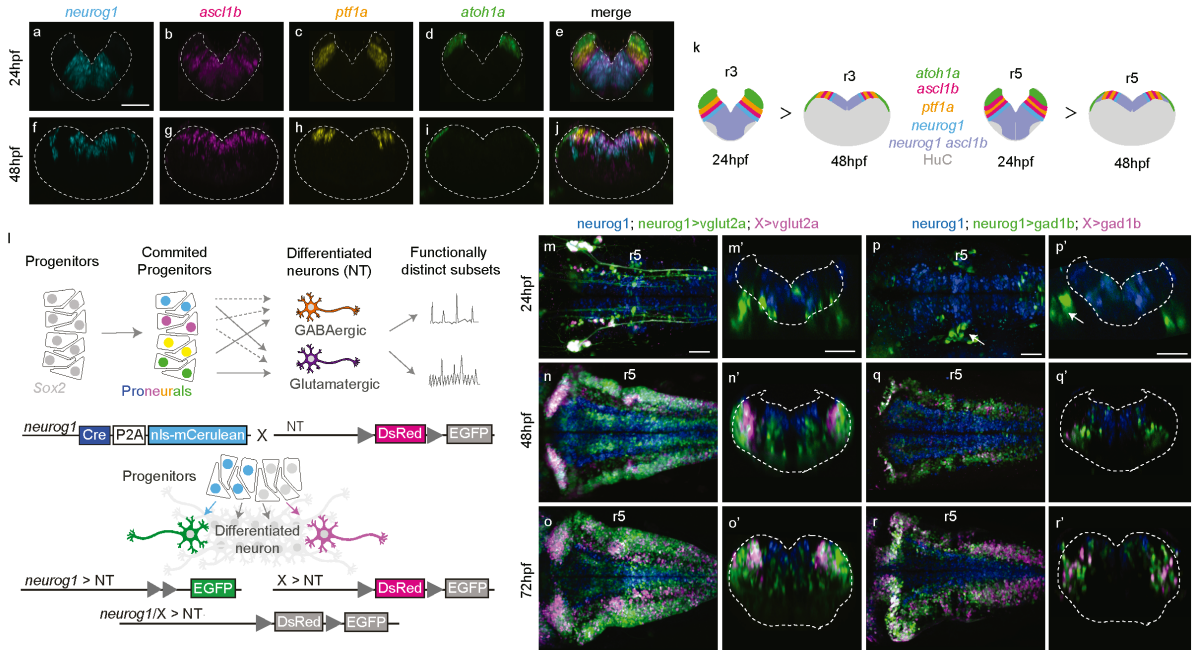

Figure 1: *neurog1*-progenitors differentially contribute to glutamatergic and GABAergic lineages.

a–j, Multiplex HCR of *neurog1, asclc1b, ptf1a* and *atoh1a* proneural genes at 24hpf (**a–e**) and 48hpf (**f–j**). Transverse views of single channels (**a–d, f–i**), and the merge of all channels (**e, j**). Note the differential expression of proneural genes along the dorsoventral (DV) axis at 24hpf and mediolateral (ML) axis at 48hpf. Transverse views through rhombomere (r) 5. **k,** Scheme summarizing the differential expression of proneural genes along the DV and ML axes of the hindbrain together with the neuronal differentiation domain (HuC) along rhombomeres 3 and 5. **l,** Scheme depicting the goal of the work, dissecting the contribution of different progenitor pools to excitatory (glutamatergic) and inhibitory (GABAergic) functional neurons, and the employed strategy to address the contribution of *neurog1*-progenitors to both neuronal lineages. **m–r, m'–r',** Temporal production of glutamatergic (**m–o**) and GABAergic (**p–r**) neurons according to the progenitor origin (*neurog1*-derivatives in green, non-*neurog1*-derivatives in magenta) at the indicated developmental times. Dorsal views with anterior to the left (**m–r**) and transverse views (**m'–r'**) through rhombomere 5. White arrows in (**p, p'**) indicates the statoacoustic sensory ganglion. hpf, hours post-fertilization; NT, neurotransmitter; r, rhombomere; X, unknown PN-expressing progenitors.

Figure 2

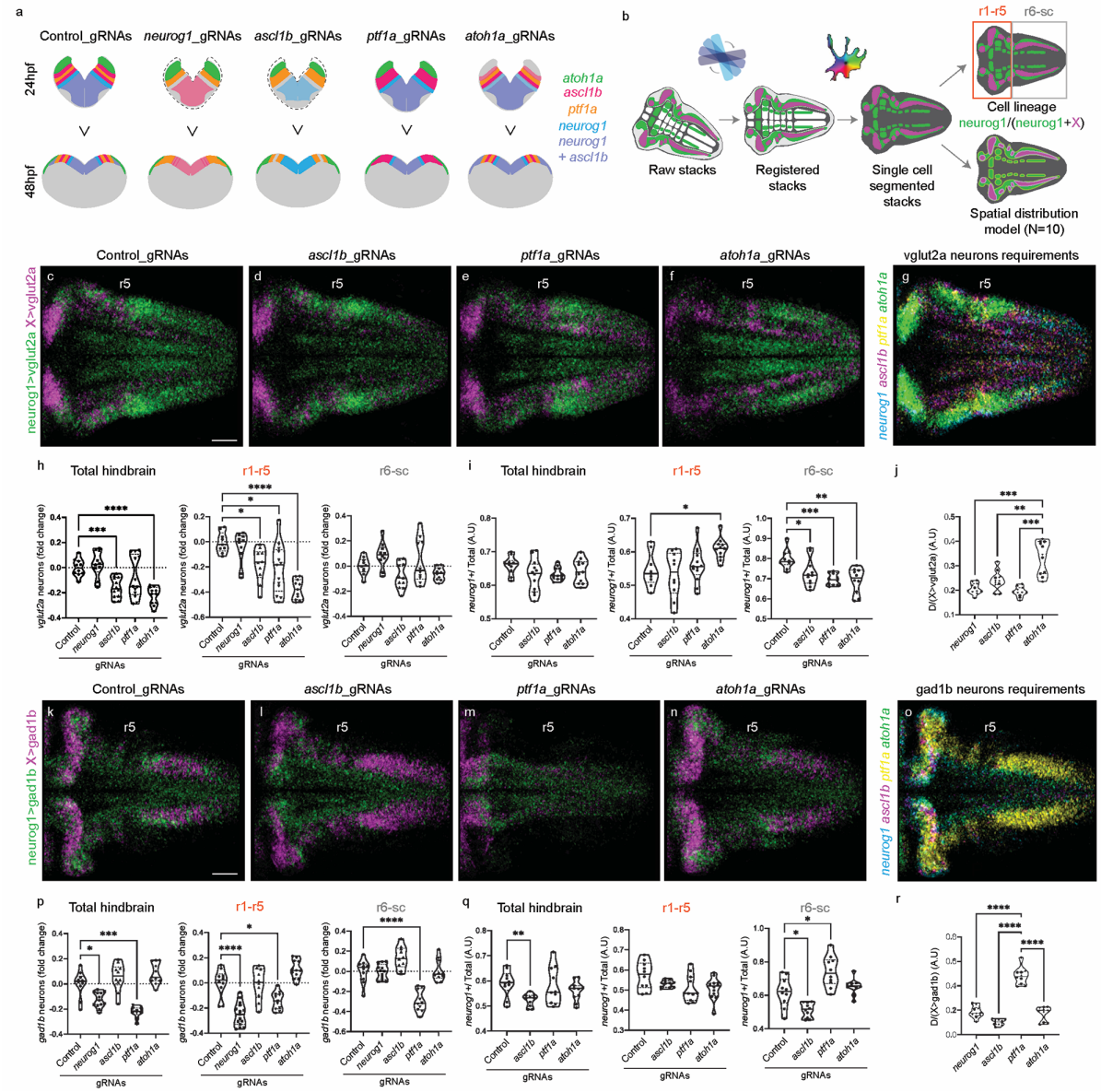

Figure 2: Glutamatergic and GABAergic lineages derive from distinct progenitor pools combinations.

a, Summary of the observed phenotypes by multiplex HCR upon proneural gene disruption (Extended Figure Data 3). **b,** Upon CRISPR-based LOF, hindbrains were imaged at 72hpf and images from 10 hindbrains per condition underwent alignment. Green (*neurog1*-derived) and magenta (non *neurog1*-derived) cells were segmented using Cellpose to *i)* quantify the proportions of glutamatergic and GABAergic neurons derived from the different progenitor populations and *ii)* construct spatial distribution 3D models allowing the evaluation of the impact of LOF on the neuronal populations across the tissue. **c–f,** Spatial distribution 3D-models of glutamatergic cells derived from *neurog1*- (green) or non-*neurog1* progenitors (magenta) upon the indicated conditions. **g,** 3D-map showing the progenitors' origin requirements for glutamatergic neurons. Note that the main contributors are *neurog1*-, *ascl1b*- and *atoh1a*-cells (see segregated progenitor Extended Data Figure 3i). **h–i,** Variation on the proportion of all glutamatergic neurons or of *neurog1*-derived glutamatergic neurons upon PN_gRNA injections with respect to the control, in the overall hindbrain (total

hindbrain), and specifically in the anterior hindbrain (r1-5) and the posterior hindbrain (r6-sc). **j,** Proportion of the non-*neurog1* derived glutamatergic neurons requirement for each of the proneural progenitor pools, measured through the intersection of control samples with the lineage requirements maps. **k–n,** Spatial distribution 3D-models of GABAergic cells derived from *neurog1*- (green) or non-*neurog1* progenitors (magenta) upon the indicated conditions. **o,** 3D-map showing the progenitors' origin requirements for GABAergic neurons. Note that the main contributors are *neurog1*-, *ptf1a*-cells (see segregated progenitor maps in Extended Data Figure 4j). **p–q,** Variation on the proportion of all GABAergic neurons or of *neurog1*-derived GABAergic neurons upon PN_gRNA injections in respect to the control, in the overall hindbrain (total hindbrain), and specifically in the anterior hindbrain (r1-5) and the posterior hindbrain (r6-sc). **r,** Proportion of the non-*neurog1* derived GABAergic neurons requirement for each of the proneurals' progenitor populations, measured through the intersection of WT samples with the lineage requirements maps. For individual sample measurements Brown-Forsythe and Welch one-way Anova tests were performed to account for variations of standard deviation and followed by Dunnett's multiple comparisons test (**h–i**; **p–q**; Table S2). For the requirement maps intersections to individual lineage traced samples a repeated measurement (RM) one-way Anova test with Geisser-Greenhouse correction was performed to account for matched dataset and was followed by a Holm-Sidak's multiple comparison test (**j, r**; Table S2). All images display dorsal views of the hindbrain with anterior to the left. r, rhombomere. *p<0.0332; **p< 0.0021 ; ***p<0.0002; ****p<0.0001

Figure 3

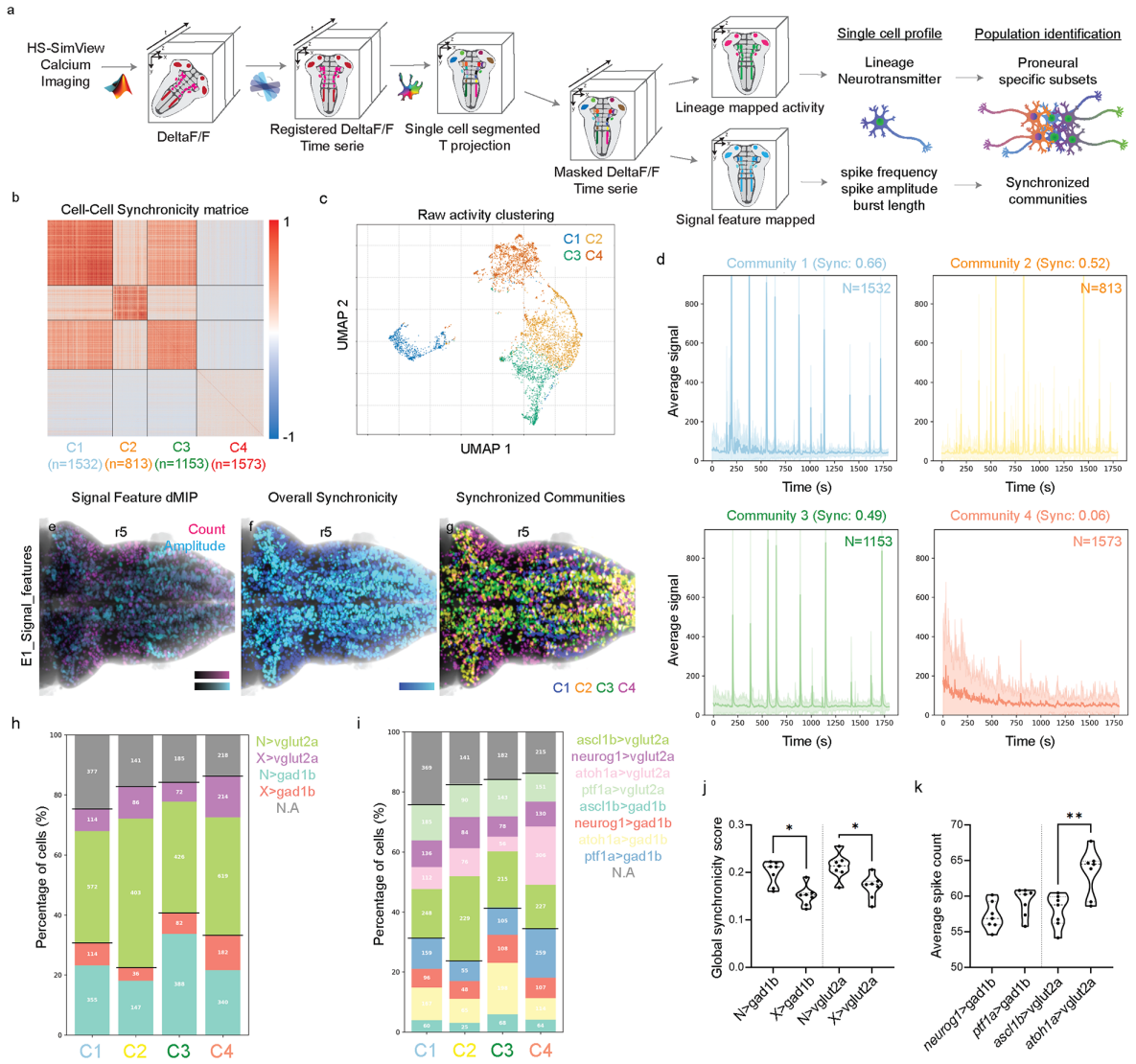

Figure 3: Functional neuronal features rely on the progenitor origin.
a, Scheme depicting the imaging and analyses pipeline: hs-SimView recordings are first processed through a series of Matlab scripts to extract the deltaF/F, and the subsequent recording is then aligned and scaled to our reference atlas using our alignment software. Aligned recordings of deltaF/F are then projected over time to obtain a 3D image representing neuron maximal activity over the time sequence. The projection is passed to Cellpose for single cell segmentation and intersected with our previously established lineage maps. Moreover, each cell's deltaF/F signal variations over the time sequence are analyzed to obtain feature maps reflecting the cells' activity characteristics. **b,** Cell-cell synchronicity matrices of hindbrain active neurons; n, number of segmented cells constituting each community. Note that we can differentiate 4 different neuronal communities (C1–C4). **c,** UMAP displaying the 4 different communities according to their synchronicity pattern. **d,** Neuronal activity profiles of C1–C4 indicating the number of analyzed cells (N) and the synchronicity score (Sync). **e–g,** 3D-maps of active neurons according to different features: count and amplitude (**e**), overall synchronicity (**f**), community belonging (**g**). **h,** Box plot displaying the cell lineage composition of C1–C4. **i,** Box plot displaying the progenitor origin requirements of C1–C4. **j,** Violin plot showing that the global synchronicity score relies on progenitor origin. **k,** Violin plot showing

that the average spike count is independent of the progenitor origin. For activity features per lineage measurements non-parametric Friedman tests were performed and followed by Dunnett's multiple comparisons test (**j–k**; Table S3). *p<0.0332; **p< 0.0021; ***p<0.0002; ****p<0.0001.

Figure 4

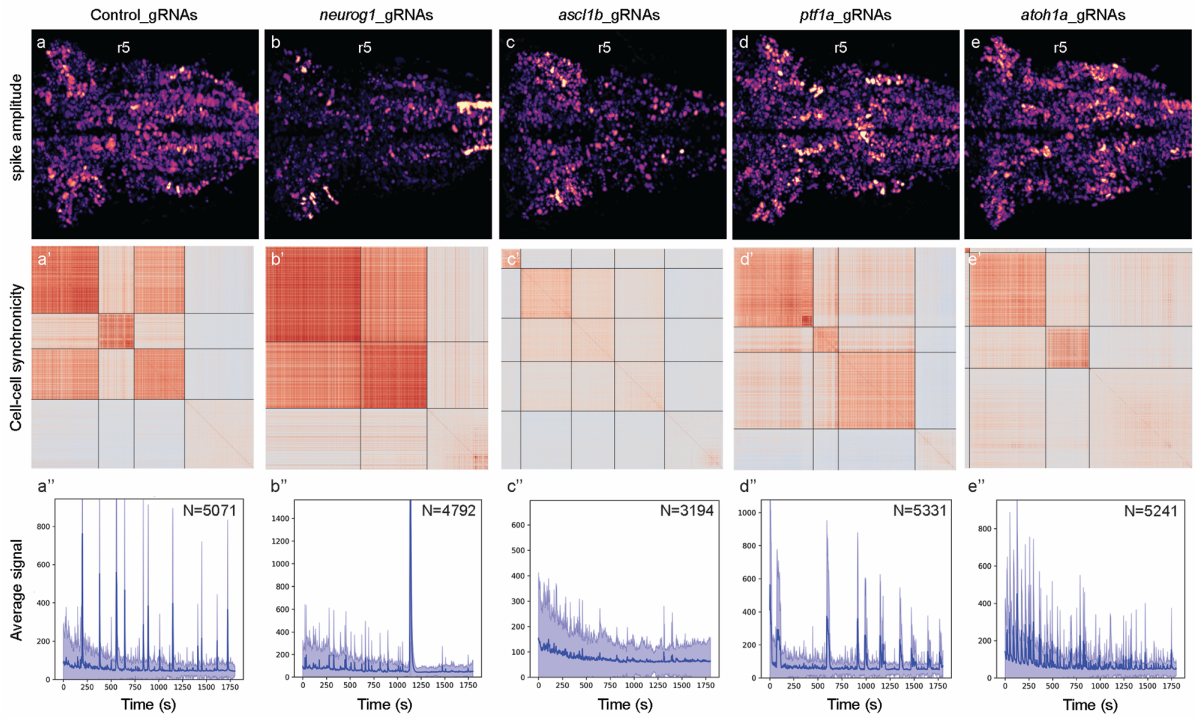

Figure 4: Disruption of specific progenitor pools results in differential changes in neuronal activity.

a–e, Neuronal activity patterns in control hindbrains and upon disruption of proneuronal progenitor pools (Extended Data Video 6–10). Dorsal views with anterior to the left. **a'–d',** Cell-cell synchronicity maps showing the 4 Louvain communities upon different conditions. **a''–d'',** Average hindbrain neuronal activity under the different conditions. Note how disruptions in the progenitor origin result in changes in community distribution and neuronal activity.

Figure 5

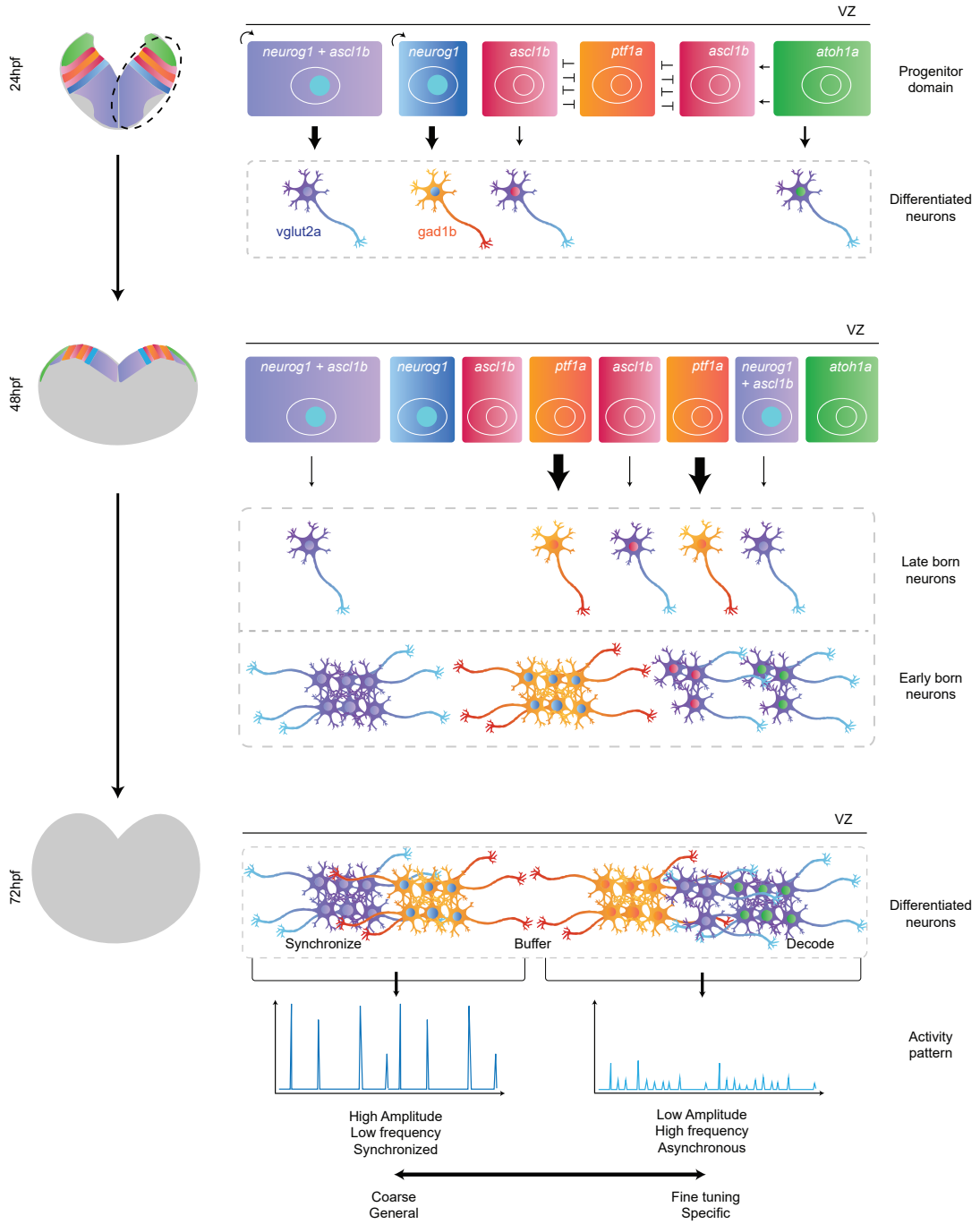

Figure 5: Progenitor origin and age are crucial parameters in establishing terminal characteristics, such as the neurotransmitter identity and function.
The neuronal progenitor domain is patterned along the DV and ML axes by differential proneural gene expression. Early on (24hpf), *neurog1*-stem cells are the first one to produce excitatory (glutamatergic, vglut2a) and inhibitory (GABAergic, gad1b) neurons with differential temporal dynamics, followed by *atoh1a*- and *ascl1b*-progenitors, which are continuously added to the glutamatergic population. On the other hand, *ptf1a*-progenitors take the relay for GABAergic neurons (48hpf). This temporally defined progenitor origin determines specific functional neuronal features: early-born medially located progenitors produce neurons characterized by high-amplitude, low-frequency, and synchronized activity, likely establishing

the baseline circuit architecture; by contrast, later-born laterally located progenitors produce neurons with low-amplitude, high-frequency, and asynchronous activity, suggesting a role in more specific fine-tuning. VZ, ventricular zone; hpf, hours post-fertilization.

EXTENDED DATA FIGURES

Extended Data Figure 1

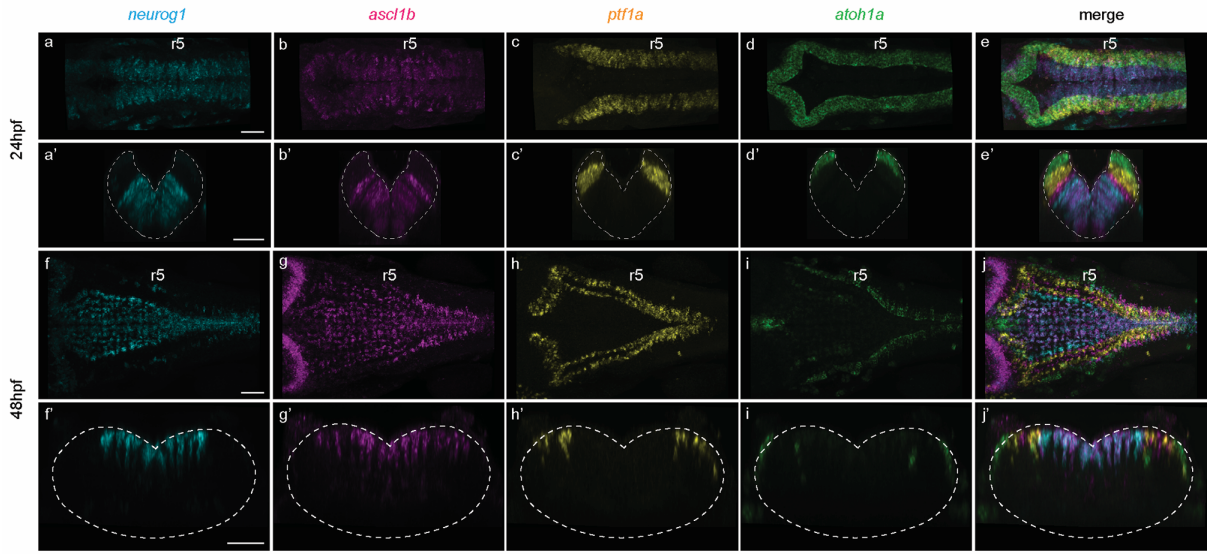

Extended Data Figure 1: Proneural genes are differentially expressed along the DV and ML axis within the hindbrain.

a–j, a'–j', Multiplex HCR of *neurog1, ascl1b*, *ptf1a*, *atoh1a* proneural genes displaying single (**a–d, f–i**) and merged (**e, j**) channels at 24hpf (**a–e, a'–e'**) and 48hpf (**f–j, f'–j'**), in dorsal (**a–j**) and transverse (**a'–j'**) views along r3. Note that proneural genes are expressed in the progenitor domain and their expression is displaced upon the growth of the below neuronal differentiation domain. r, rhombomere; hpf, hours post-fertilization.

Extended Data Figure 2

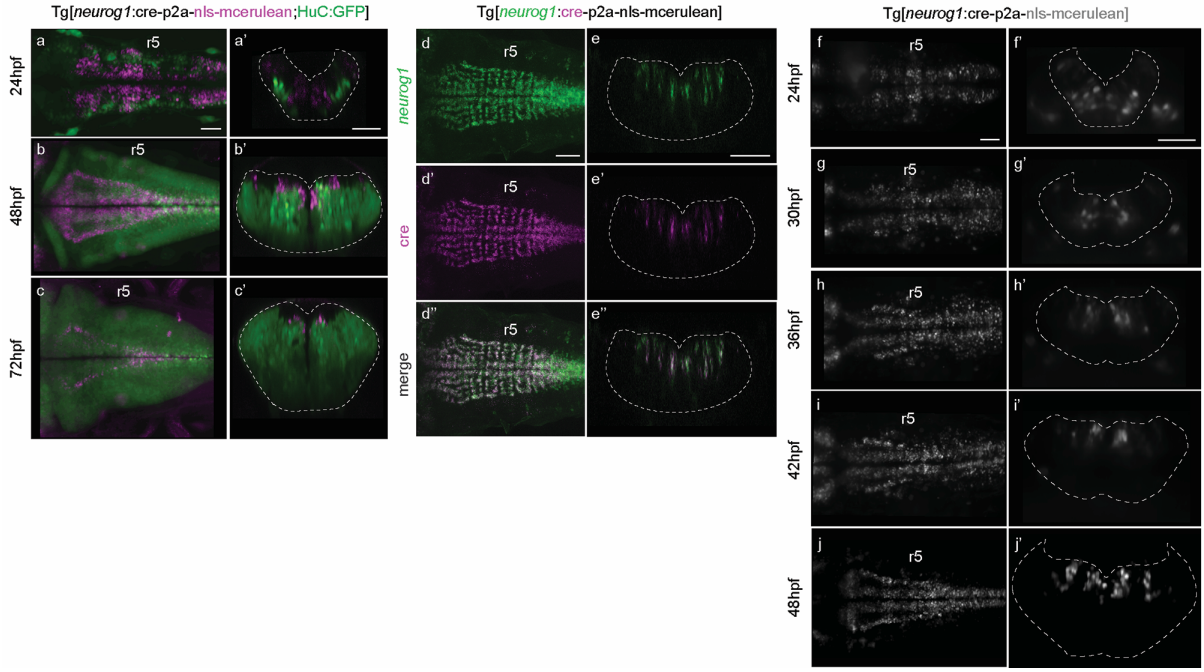

Extended Data Figure 2: Characterization of the Tg[neurog1:Cre-P2A-nls-Cerulean] fish line. a–c, a'–c', Double transgenic Tg[neurog1:Cre-P2A-nls-Cerulean; HuC:GFP] embryos at the indicated developmental times. Dorsal maximal intensity projection (MIP) (**a–c**) and transverse section through rhombomere 5 (**a'–c'**). Note that neurog1-Cerulean expression in magenta is restricted to the progenitor domain. **d–d'', e–e'',** HCR for *neurog1* and *Cre* in Tg[neurog1:Cre-P2A-nls-Cerulean] embryos at 40hpf. Note that *Cre*-positive cells overlap with *neurog1*-cells. **f–j, f'–j',** Stills from a time-lapse video showing the expression of Cerulean protein recapitulates the dynamics of *neurog1* expression[23]. Note the stability of Cerulean protein, which is maintained in neurons deriving from *neurog1*-cells (see red asterisk). **a–c, d–d'', f–j**, Dorsal views with anterior to the left. **a'–c', e–e'', f'–j'**, Transverse views through rhombomere 5. r, rhombomere; hpf, hours post-fertilization.

Extended Data Figure 3

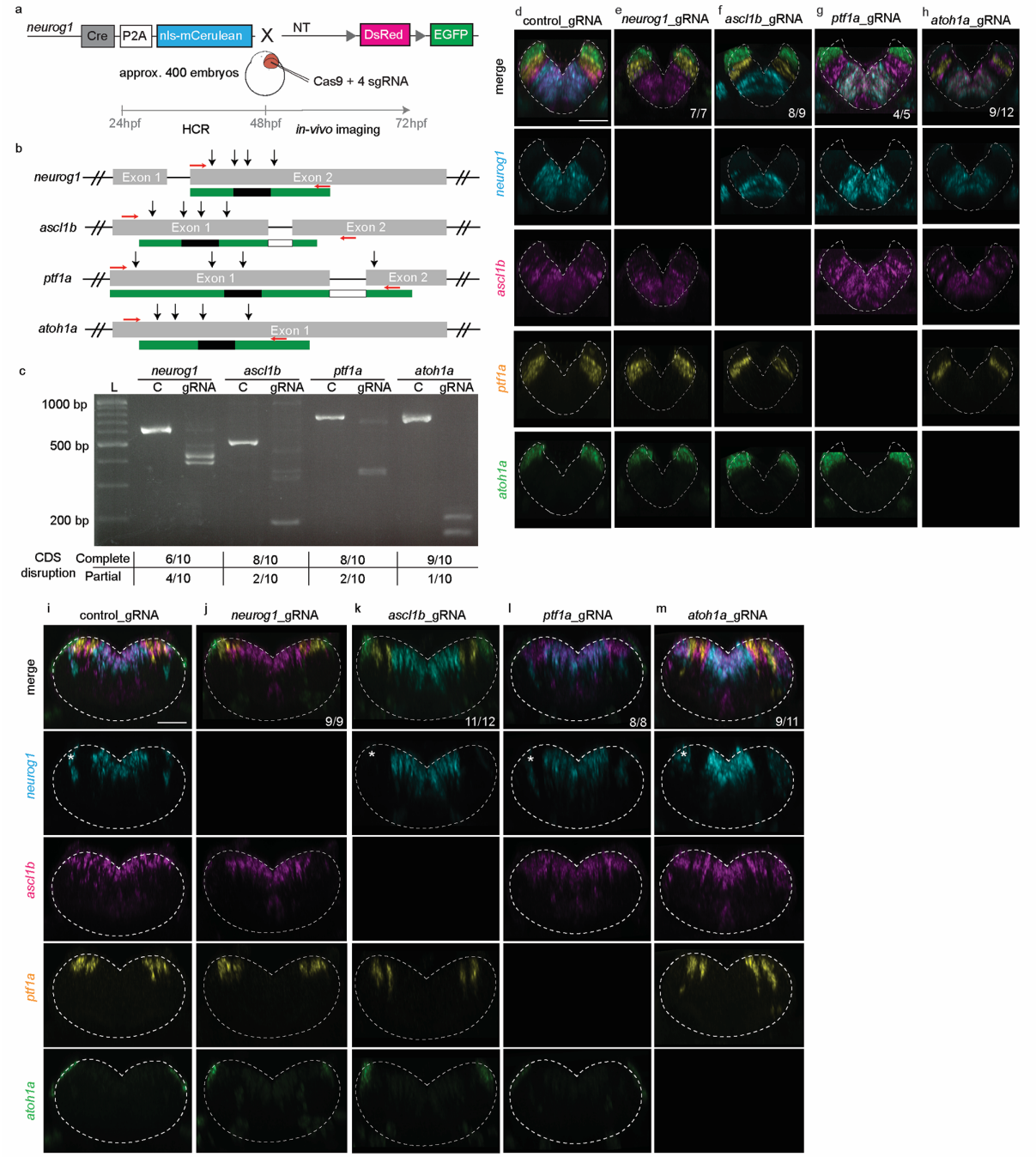

Extended Data Figure 3: CRISPR-based loss-of-function approach.
a, Scheme depicting the CRISPR/Cas9-based approach that produces loss-of-function (LOF) phenotypes in F_0. Tg[neurog1:Cre:*vglut2a*/*gad1b*:switch] embryos were injected with control or 4 different gRNAs for a single proneural gene (PN_gRNAs) and they were let to develop until 24hpf and 48hpf for HCR proneural gene expression analysis, and 72hpf for cell lineage studies (Figure 2). **b,** Strategy for the proneural gene gRNAs design. Black arrows indicate the position of the 4 gRNAs within the corresponding proneural gene. Red arrows indicate the position of the PCR primers used for genotyping. **c,** Genotyping of PN_gRNAs injected embryos. gDNA from single embryos injected with control (C) of PN_gRNAs (gRNA) were used for genotyping (see Methods). Agarose gel displaying the amplified bands. The number of embryos displaying

complete or partial disruption of the amplified coding sequence (CDS) after PN-gRNAs injection is indicated in the table. Efficiency of the gene disruption was assessed in single embryos at F_0. **d–h, i–m**, Multiplex HCR of *neurog1, asclc1b, ptf1a* and *atoh1a* proneural genes at 24hpf and 48hpf, respectively, upon control (**d, i**) or PN-gRNA injection (**e–h, j–m**). Transverse views through rhombomere 5 displaying the indicated single channel or the merge of them. White asterisk in the *neurog1*- profiled embryos (**i–m**) indicate the loss of expression of *neurog1*- in the most lateral domain of expression upon *ascl1b* loss-of-function.

Extended Data Figure 4

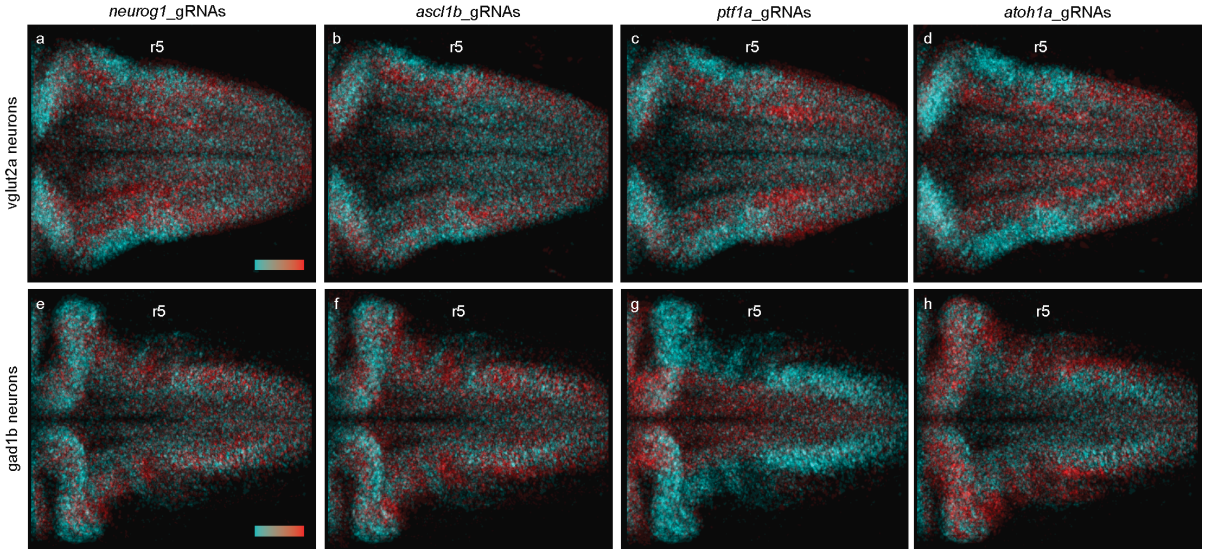

Extended Data Figure 4: Differential requirement of progenitor pools for glutamatergic and GABAergic lineages.

a–f, 3D-maps displaying the progenitor origin requirement (hue legend cyan) and compensation (hue legend red) for glutamatergic (**a–d**) and GABAergic (**e–h**) neurons. Note that the main progenitor's requirements for glutamatergic neurons are *ascl1b*- (medial) and *atoh1a*-(lateral), whereas to the GABAergic neurons are *ptf1a*-progenitors. All images display dorsal MIP with anterior to the left. r, rhombomere.

Extended Data Figure 5

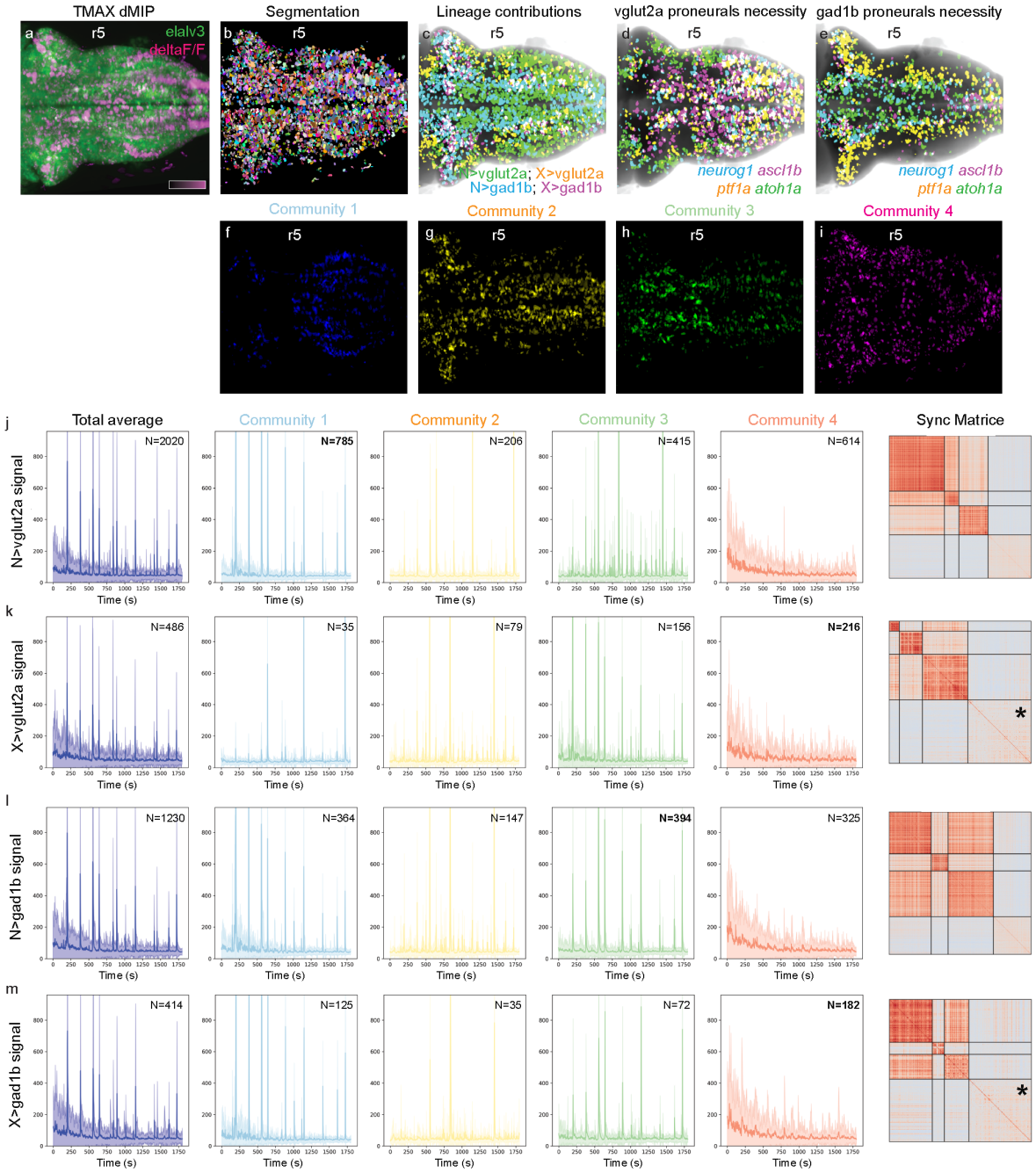

Extended Data Figure 5: Mapping lineage origin and functional activity features to a common hindbrain 3D reference map.

a, Dorsal view of Tg[*elavl3*:jrGECO1b] embryo upon Ca^{++}-recording within a 72hpf hindbrain (Extended Data Video 6). **b,** Dorsal view displaying all active segmented neurons. **c,** 3D-map displaying the contribution of *neurog1*-progenitors (green and cyan cells) and non *neurog1*-progenitors (yellow and magenta cells) to glutamatergic (green and yellow) and GABAergic (cyan and magenta) lineages. **d–e,** 3D-maps of the proneural gene requirements for glutamatergic (**d**) and GABAergic (**e**) lineages. **f–m**, 3D-maps of active neurons belonging to the different communities (C1–C4). **j–k,** Neuronal activity profiles of all glutamatergic (**j–k**) and GABAergic (**l–m**) cells (total average) and segregated by community belonging (C1–C4) from

neurog1-progenitors (**j, l**) or non *neurog1*- progenitors (**k, m**) with the corresponding cell synchronicity matrix. **a–i,** Images display dorsal views with anterior to the left.

EXTENDED DATA VIDEOS

Extended Data Video 1

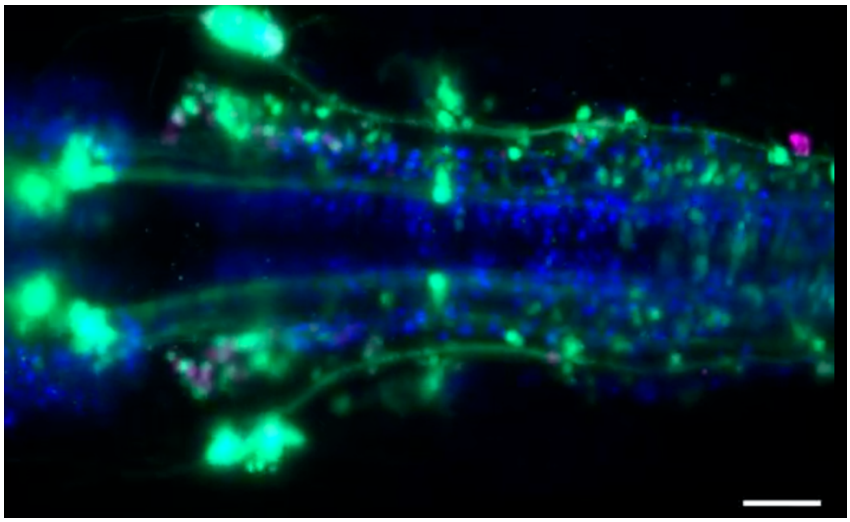

Extended Data Video 1: *neurog1*-population produces glutamatergic neurons at very early stages.
Tg[neurog1:Cre:*vglut*:switch] embryo was imaged from 24hpf until 48hpf using LSFM. Note that *neurog1*-progenitors express Cerulean and when they differentiate into glutamatergic neurons, they start expressing GFP (green), whereas the rest of glutamatergic neurons express DsRed (magenta).

Extended Data Video 2

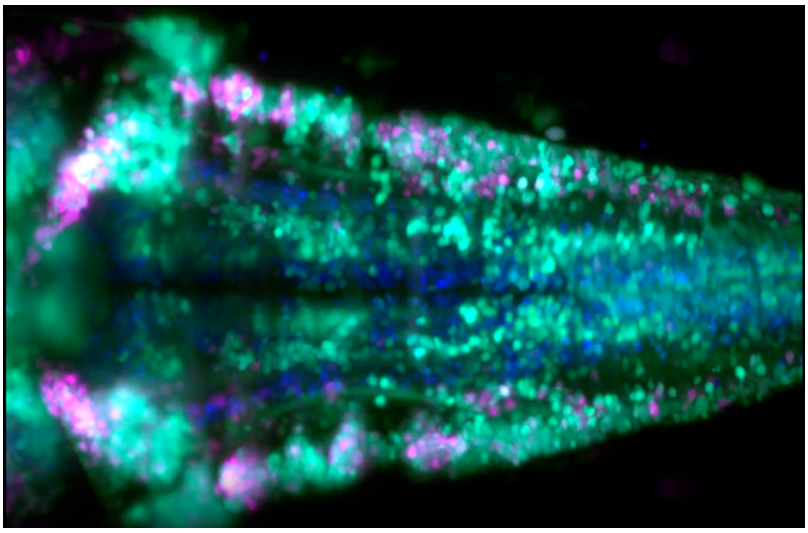

Extended Data Video 2: *neurog1*-population and other progenitor pools contribute to glutamatergic neurons at later stages.
Tg[neurog1:Cre:*vglut*:switch] embryo was imaged from 48hpf until 72hpf using LSFM. Note that *neurog1*-progenitors express Cerulean and when they differentiate into glutamatergic neurons, they start expressing GFP (green), whereas the rest of glutamatergic neurons express DsRed (magenta).

Extended Data Video 3

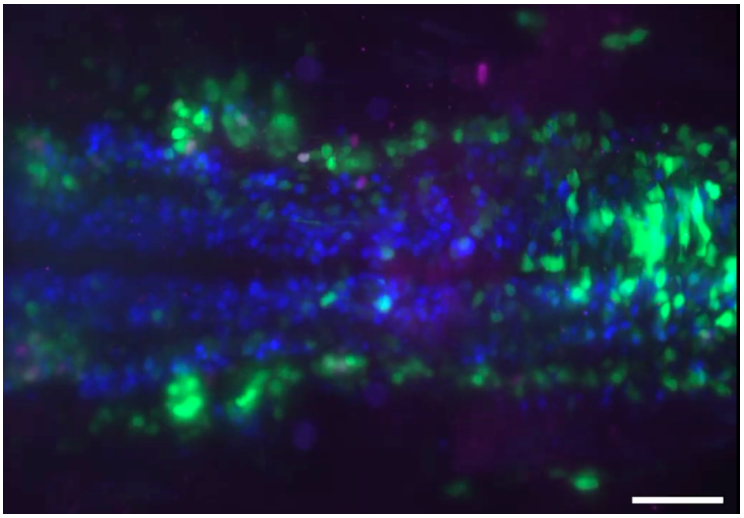

Extended Data Video 3: *neurog1*-population produces GABAergic neurons at early stages. Tg[neurog1:Cre:*gad1b*:switch] embryo was imaged from 24hpf until 48hpf using LSFM. Note that *neurog1*-progenitors express Cerulean and when they differentiate into GABAergic neurons, they start expressing GFP (green), whereas the rest of GABAergic neurons express DsRed (magenta).

Extended Data Video 4

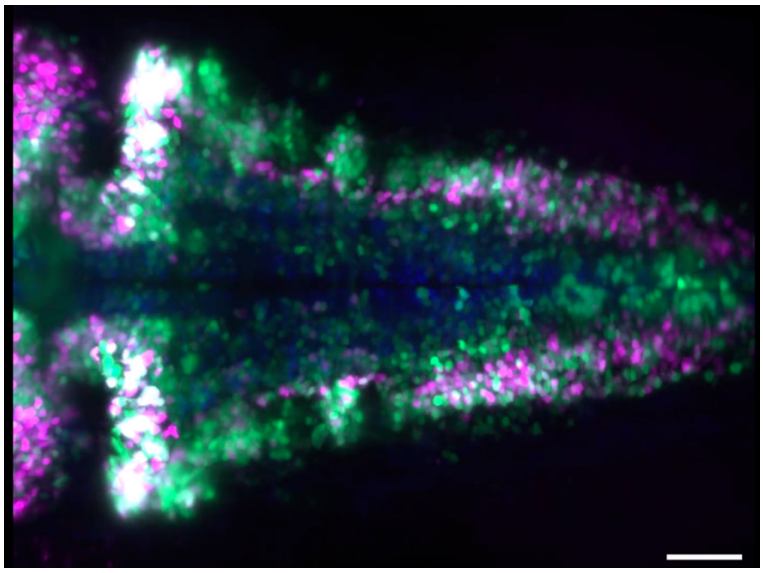

Extended Data Video 4: *neurog1*-population produces GABAergic neurons at early stages. Tg[neurog1:Cre:*gad1b*:switch] embryo was imaged from 48hpf until 72hpf using LSFM. Note that non *neurog1*-progenitors (magenta cells) take the relay of *neurog1*-progenitors in the production of GABAergic neurons.

Extended Data Video 5

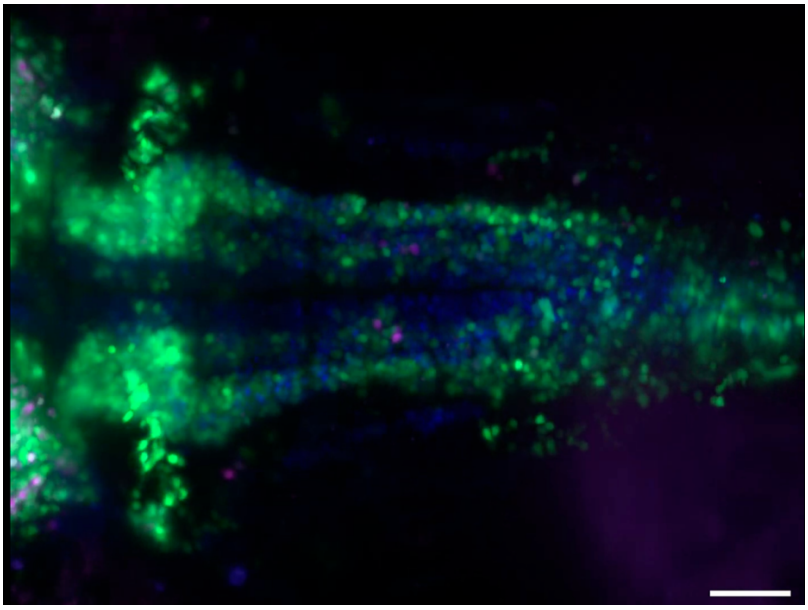

Extended Data Video 5: GABAergic neurons are generated independently of *ptf1a*.
Tg[neurog1:Cre:*gad1b*:switch] embryo injected with 4 different gRNAs for *ptf1a* imaged from 48hpf until 72hpf using LSFM. Note that indeed *neurog1*-cells (cerulean) give rise to GABAergic neurons (green) in the absence of *ptf1a.*

Extended Data Video 6

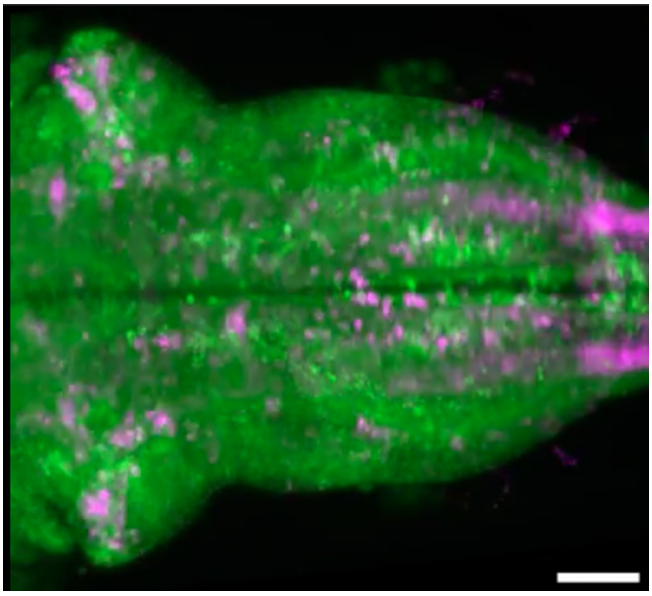

Extended Data Video 6: Neuronal activity pattern in the hindbrain in control embryos. Calcium recordings in Tg[*elavl3*:jrGECO1b] embryos at 72hpf after control gRNA injections. Dorsal view with anterior to the left.

Extended Data Video 7

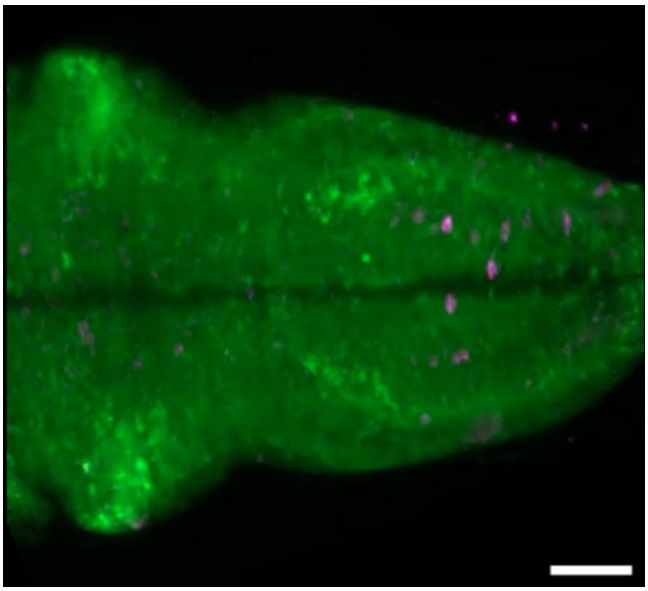

Extended Data Video 7: Neuronal activity pattern in the hindbrain upon disruption of *neurog1*-progenitors.
Calcium recordings in Tg[*elavl3*:jrGECO1b] embryo at 72hpf after *neurog1*-gRNA injections. Note how the Ca^{++}-activity pattern changes upon disruption of *neurog1*-progenitors. Dorsal view with anterior to the left.

Extended Data Video 8

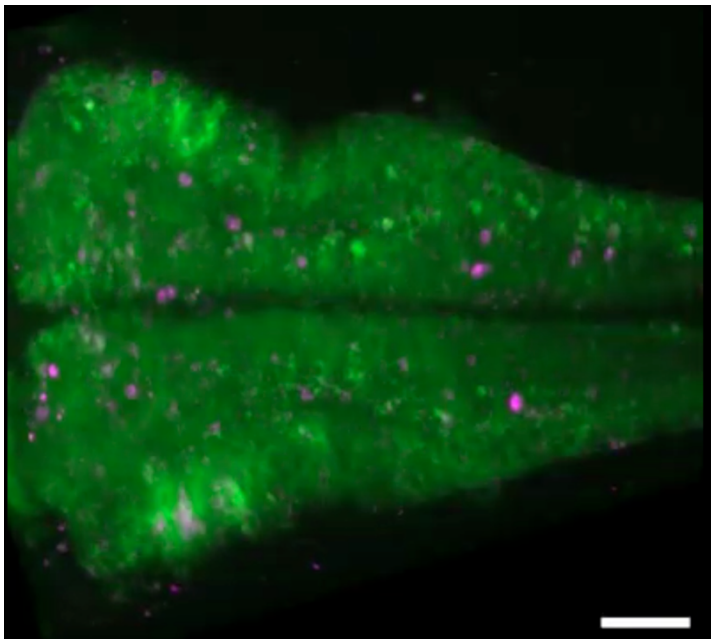

Extended Data Video 8: Neuronal activity pattern in the hindbrain upon disruption of *ascl1b*-progenitors.
Calcium recordings in Tg[*elavl3*:jrGECO1b] embryo at 72hpf after *ascl1b*-gRNA injections. Note how the Ca^{++}-activity pattern changes upon disruption of *ascl1b*-progenitors. Dorsal view with anterior to the left.

Extended Data Video 9

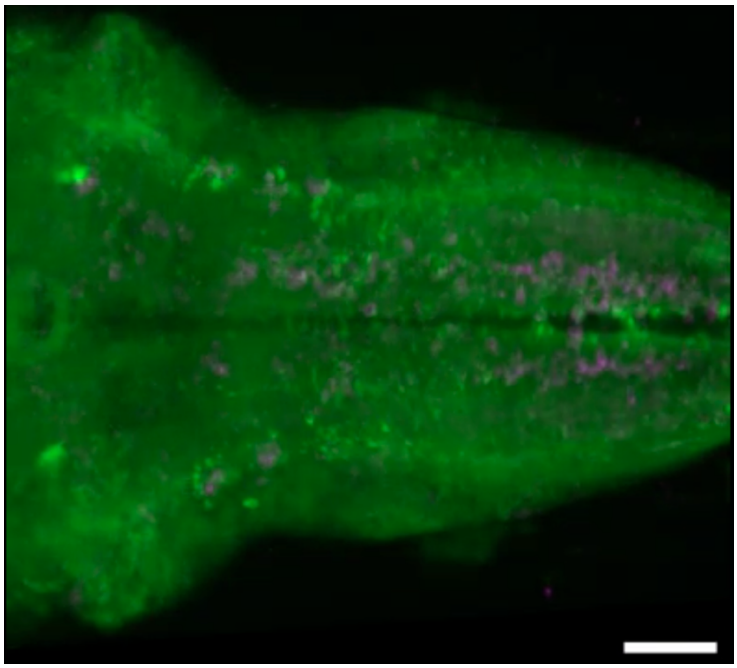

Extended Data Video 9: Neuronal activity pattern in the hindbrain upon disruption of *ptf1a*-progenitors.
Calcium recordings in Tg[*elavl3*:jrGECO1b] embryo at 72hpf after *ptf1a*-gRNA injections. Note how the Ca^{++}-activity pattern changes upon disruption of *ptf1a*-progenitors. Dorsal view with anterior to the left.

Extended Data Video 10

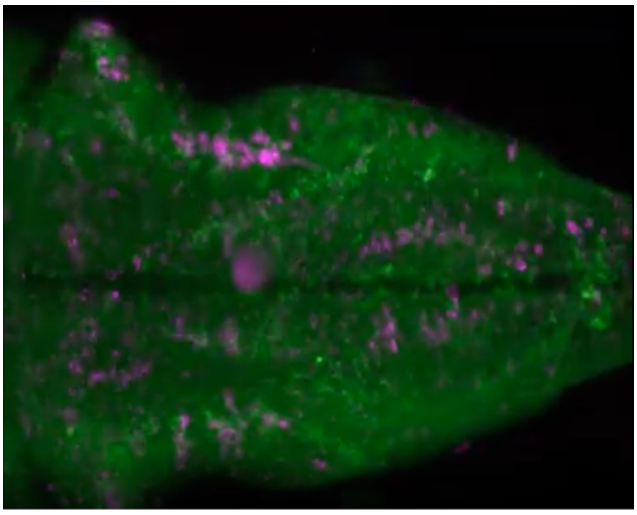

Extended Data Video 10: Neuronal activity pattern in the hindbrain upon disruption of *atoh1a*-progenitors.
Calcium recordings in Tg[*elavl3*:jrGECO1b] embryo at 72hpf after *atoh1a*-gRNA injections. Note how the Ca^{++}-activity pattern changes upon disruption of *atoh1a*-progenitors. Dorsal view with anterior to the left.